THE R-MATRIX BOOTSTRAP

by

Harish Murali

A Thesis

Submitted to the Faculty of Purdue University

In Partial Fulfillment of the Requirements for the degree of

Master of Science

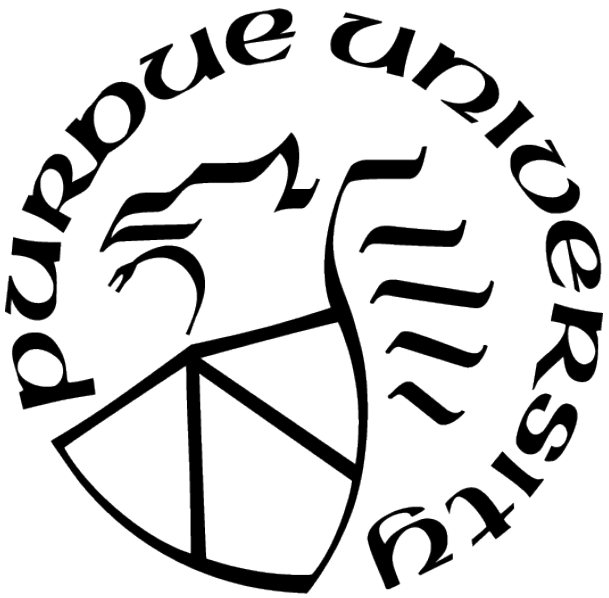

Department of Physics and Astronomy

West Lafayette, Indiana

May 2021

THE PURDUE UNIVERSITY GRADUATE SCHOOL
STATEMENT OF COMMITTEE APPROVAL

Dr. Martin Kruczenski, Chair

Dept. of Physics and Astronomy

Dr. Nima Lashkari

Dept. of Physics and Astronomy

Dr. Sergei Khlebnikov

Dept. of Physics and Astronomy

Approved by:

Dr. John P. Finley

ACKNOWLEDGMENTS

I'm extremely grateful to Martin for his constant guidance and support. I really appreciate the effort and time he's invested in me, sometimes spending hours debugging my code. I'd also like to thank my committee members Nima and Sergei for taking the time out for my defense. I'm deeply indebted to the faculty at the Dept. of Physics and Astronomy, especially Martin, Sergei and Nima, for teaching me so much of the physics I know. Finally, I'd like to thank my friends and family for their emotional support throughout grad school.

TABLE OF CONTENTS

LIST OF FIGURES

ABSTRACT

In this thesis, we extend the numerical S-matrix bootstrap program to 1+1d theories with a boundary, where we bootstrap the $1 \to 1$ reflection matrix (R-matrix). We review the constraints that a physical R-matrix must obey, namely unitarity, analyticiy and crossing symmetry. We then carve out the allowed space of 2d R-matrices with the $O(N)$ nonlinear sigma model and the periodic Yang Baxter solution in the bulk. We find a variety of integrable R-matrices along the boundary of the allowed space both with and without free parameters. The integrable models without a free parameter appear at vertices of the allowed space, while those with a free parameter occupy the whole boundary. We also introduce the extended analyticity constraint where we increase the domain of analyticity beyond the physical region. In some cases, the allowed space of R-matrices shrinks drastically and we observe new vertices which correspond to integrable theories. We also find a new integrable R-matrix through our numerics, which we later obtained by solving the boundary Yang–Baxter equation. Finally, we derive the dual to the extended analyticity problem and find that the formalism allows for R-matrices which do not saturate unitarity to lie on the boundary of the allowed region.

1. INTRODUCTION

The S-matrix Bootstrap is an ambitious program from the 60s, which aimed to obtain the exact S-matrix of strong nuclear interactions [1], starting only from some simple axioms that all physical theories are expected to obey, thereby bypassing a field theoretic description of the subatomic particles. However, with the advent of Quantum Chromodynamics which very successfully described the physics of strong interactions, the S-matrix bootstrap program was shelved. Recently, motivated by progress in bootstrapping CFTs, the S-matrix bootstrap was revisited in [2]. Since then, there has been a lot of interesting and promising work in this direction. The basic idea is to use computers to carve out the space of S-matrices which satisfy the constraints of unitarity, analyticity, and crossing symmetry. This problem can be posed as a constrained convex optimization problem which has been studied very well in the literature and can be solved by very fast algorithms. This is a powerful probe of nonperturbative physics that uses simple numerics.

In the seminal works [2], [3], the authors addressed the following question - given a spectrum of massive particles in $1+1$ dimensions, what is the largest possible coupling to bound states that one can have? The intuition is that as the coupling grows, more states from the continuum can be pulled down as bound states, and so, for a fixed spectrum, there exists a maximal coupling. Surprisingly, the class of theories which maximize this coupling turned out to be a subsector of the integrable Sine-Gordon model. In [4] and [5], this idea of maximizing couplings was applied to theories in higher dimensional and with multiple amplitudes respectively.

Another problem that we can consider in this context is to look at sections of the infinite dimensional space of allowed S-matrices that satisfy all the constraints. We can then study the boundary of such sections where one often encounters special theories as vertices. In [6], the 2d $O(N)$ bosonic S-matrix, without any bound states was bootstrapped. In that paper, the authors show that the integrable $O(N)$ non-linear sigma model (NLSM), which was first studied in [7] and exactly solved in [8], lies at a vertex of the space of allowed S-matrices. This agrees with our intuition that integrable models without free parameters, being highly constrained, must occupy distinguished points in the space of theories. In subsequent work

[9], it was shown that the allowed space of $O(N)$ symmetric S-matrices has two other vertices that correspond to the free theory and another integrable S-matrix called the periodic Yang Baxter (pYB) solution. In related work [10], it was shown that when an integrable theory has a free parameter, it can show up along a segment of the boundary, instead of at a vertex.

In [9], the convex dual of the S-matrix bootstrap problem was studied, which provides a way to rewrite a convex maximization problem as a minimization problem. This is particularly useful in scenarios where the convergence is poor with increasing resolution, because it allows us to place upper bounds on the answer. In [11], the dual formulation for 3+1d scattering amplitudes was presented, and the authors demonstrate that the dual problem has better convergence even with fewer variables.

Two of the biggest unsolved problems in theoretical particle physics are quantization of gravity and analytic description of the low energy physics of QCD. Both of these problems are currently being studied using the S-matrix bootstrap. In [12], bounds were obtained on the couplings in the low energy effective Lagrangian of worldsheet excitations of confining strings using the S-matrix bootstrap approach. The 3+1d pion scattering amplitude was studied in [13] and interesting features were observed in the scattering lengths and chiral zero positions. In [14], precise bounds were obtained on the low energy effective Lagrangian in consistent UV complete theories which have a graviton. In [15], a lower bound on the coupling constant for the leading correction to the maximal supergravity action. There have been a plethora of other works on the S-matrix bootstrap that incorporate spin, consider field theories with various symmetry groups, supersymmetry, etc [16]–[31]. The S-matrix bootstrap is clearly a very useful tool to study both highly symmetric, theoretically interesting models and also more down to earth questions about the real world.

In this work, motivated by these results, we extend the S-matrix bootstrap to the case of QFTs with a boundary, which are an important class of theories that show up in many areas of theoretical physics. Specifically, we bootstrap the reflection matrix (R-matrix) for a given integrable bulk S-matrix. As in the case of the S-matrix bootstrap, we have certain unitarity, crossing and analyticity constraints that the R-matrix must obey. One important difference is that we have a non-trivial crossing equation which involves the bulk S-matrix and thus crossing is a nonlinear constraint if the S-matrix is allowed vary. In this thesis, we

fix the S-matrix to two cases - $O(N)$ NLSM and the pYB solution. An obvious direction for future work would be to bootstrap both the bulk and boundary scattering amplitudes together. We obtain an interesting result that integrable R-matrices for the $O(N)$ model without any free parameters lie at vertices of the allowed space, and those with a free parameter appear as 1 dimensional segments along the boundary. Another result we present is the exact R-matrix for the pYB solution, which has not been worked out previously to our knowledge. Interestingly, we first found this R-matrix numerically and then obtained the analytic expression by solving the boundary Yang-Baxter equation.

This thesis is organized as follows - in sections 2, 3, we define the S-matrix and the R-matrix and describe the constraints that they must satisfy. We then quote exact results from the literature which were obtained using integrability. We also derive a new result - the diagonal R-matrix for the pYB solution. In section 4, we describe our numerical procedure and how we can use convex optimization to solve the bootstrap. We then introduce the notion of convex duality. In the next section, we present the results of the numerical bootstrap. In section 6, we present an alternative derivation of the dual problem and show that we can have theories which do not saturate unitarity along the boundary of the allowed regions. We present our conclusions in section 7. The Python code for the numerics is included in appendix C.

2. THE S-MATRIX - CONSTRAINTS AND EXACT RESULTS

Before we formally define the S-matrix, we first need to define asymptotic in and out states in interacting theories. In states are those which have a well defined particle number and particle momentum at time $t = -\infty$. These generically evolve into non-trivial states in an interacting field theory at time $t = +\infty$. Similarly, we define asymptotic out states as those which have a well defined particle number and particle momentum at time $t = +\infty$. Again, these evolve from non-trivial states at $t = -\infty$. Now, the S-matrix elements are defined as overlaps of the asymptotic in and out states as follows

$$S_{a_1,a_2,\dots}^{b_1,b_2,\dots}(p_{a_1}, p_{b_1}, \dots) = {}^{\text{out}}\langle b_1, p_{b_1}; b_2, p_{b_2}; \dots | a_1, p_{a_1}; a_2, p_{a_2}; \dots \rangle^{\text{in}} \ , \tag{2.1}$$

where p_{i} are the momenta of the in and out particles, and the indices a_{i} and b_{i} label any additional quantum numbers in the theory. We will only be considering $2 \to 2$ scattering of identical particles in 2d, which leads to certain simplifications. It will be convenient to parameterize the on shell momenta $p = (\varepsilon, k)$ using a rapidity variable θ as follows

$$\varepsilon = m\cosh(\theta) \ , \tag{2.2a}$$

$$k = m\sinh(\theta) \ , \tag{2.2b}$$

where m is the mass of the particles. The S-matrix being an observable, can only depend on Lorentz invariant quantities. For $2 \to 2$ S-matrices, these are the Mandelstam invariants which are defined as

$$s = (p_1 + p_2)^2 = (p_3 + p_4)^2 \ , \tag{2.3}$$

$$t = (p_1 - p_3)^2 = (p_2 - p_4)^2 \ , \tag{2.4}$$

$$u = (p_1 - p_4)^2 = (p_2 - p_3)^2 \ . \tag{2.5}$$

Conservation of momentum in 1+1d QFTs implies that we must have either $t = 0$ and $u = 4m^2 - s$, or $u = 0$ and $t = 4m^2 - s$, depending on how we chose to label the particles.

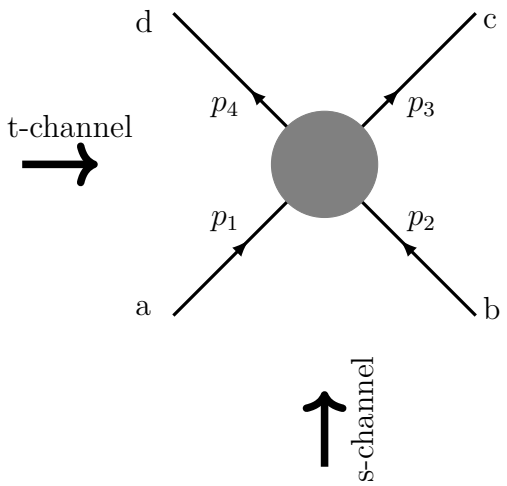

Figure 2.1. The s-channel amplitude is the same as the t-channel amplitude when analytically continued to the point $4 - s$. This is trivially true in individual Feynman diagrams, but can also be shown nonperturbatively using the LSZ reduction formula.

One can check this straightforwardly by going to the center of mass frame. So, the S-matrix is only a function of the Mandesltam s variable. It is also useful to note that

$$s = 4m^2 \cosh^2\left(\frac{\theta_1 - \theta_2}{2}\right) \ . \tag{2.6}$$

This makes manifest the fact that physical scattering states have $s \geq 4m^2$. Putting all this together, we have the following definition of the $2 \to 2$ S-matrix

$$S_{ab}^{cd}(\theta_1 - \theta_2) = \ {}^{\text{out}}\langle c, \theta_1; d, \theta_2 | a, \theta_1; b, \theta_2 \rangle^{\text{in}} \ . \tag{2.7}$$

The S-matrix of unitary QFTs must obey an important constraint namely, the sum of probabilities add to unity. Following the simple argument in [6], consider unitarity constraint on the full multiparticle S-matrix

$$\mathbb{S}\mathbb{S}^\dagger = \mathbb{I} \ , \tag{2.8}$$

where $\mathbb{I}$ is the identity operator in the appropriate dimensions. Now consider the 2 particle subsector D spanned by some set $\{|\psi_\alpha\rangle\}$. We have

$$\sum_{|\psi_\beta\rangle} \langle\psi_\alpha|\mathbb{S}|\psi_\beta\rangle \langle\psi_\beta|\mathbb{S}^\dagger|\psi_\alpha\rangle = 1 \ , \tag{2.9}$$

$$\sum_{|\psi_\beta\rangle\in D} \langle\psi_\alpha|\mathbb{S}|\psi_\beta\rangle \langle\psi_\beta|\mathbb{S}^\dagger|\psi_\alpha\rangle + \sum_{|\psi_\beta\rangle\notin D} \langle\psi_\alpha|\mathbb{S}|\psi_\beta\rangle \langle\psi_\beta|\mathbb{S}^\dagger|\psi_\alpha\rangle = 1 \ . \tag{2.10}$$

The second term of the last equation is clearly a non-negative quantity. So, the S-matrix restricted to a subspace D satisfies the following semidefiniteness constraint

$$S_D S_D^\dagger \preccurlyeq \mathbb{I} \ . \tag{2.11}$$

A crucial consequence of relativistic invariance in field theories is crossing symmetry. In 2-to-2 scattering, crossing is an equivalence between the S-matrix in the s-channel and in the t-channel as illustrated in fig.2.1. One can show that crossing is a symmetry of scattering amplitudes using the LSZ reduction formula which can be found in any standard text on QFTs. For 2d S-matrices, this implies

$$S_{ab}^{cd}(s) = S_{\bar{d}a}^{\bar{b}c}(t = 4m^2 - s) \ . \tag{2.12}$$

Now, we consider in brief the analyticity of the S-matrix. Just as in nonrelativistic scattering, when the S-matrix is analytically continued beyond the physical scattering region, the poles we encounter indicate the presence of resonances and bound states. Bound states correspond to subthreshold poles ($s < 4m^2$), while complex poles correspond to Breit-Wigner resonances.

Apart from these, field theory amplitudes have one other source of non-analyticity, namely the threshold branch cuts. In perturbation theory, we can see that individual Feynman diagrams have branch cuts via the Cutkosky cutting rules which evaluate the discontinuity across said branch cuts with a simple prescription. However, it can also be shown non-perturbatively that whenever intermediate particles in a scattering process have sufficient energy to go on shell (the inelastic threshold), a branch cut is opened up (for a simple

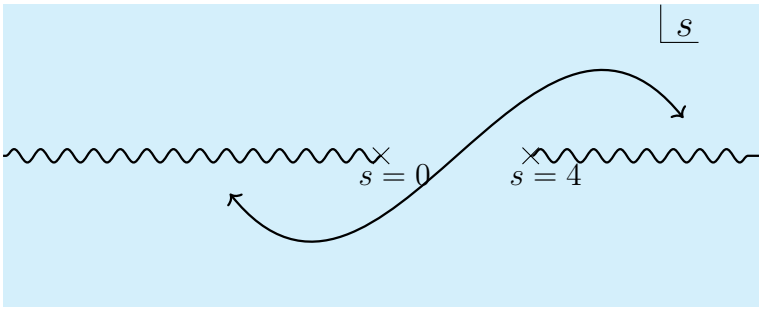

Figure 2.2. The physical S-matrix is the boundary value of an analytic function with threshold branch cuts running from $s = 4$ to ∞, and a corresponding crossed cut from $t = 4$ (i.e. s=0) to ∞. The arrow indicates crossing symmetry of the S-matrix from $s \to 4 - s$.

explanation, see chapter 1 of [1]). So, in our case of 2-to-2 scattering in 2d, we have a branch cut running from $s = 4m^2$ to ∞. The physical S-matrix is defined as the boundary value of an analytic function in the following way

$$\mathbb{S}^{\text{phys}}(s) = \lim_{\epsilon \to 0} \mathbb{S}(s + \mathrm{i}\epsilon) \ . \tag{2.13}$$

There can also be branch cuts at other particle production thresholds such as $s = 9m^2, 16m^2, \ldots$ which correspond to more number of particles going on shell. Note that crossing symmetry requires crossed branch cuts running from $s = 0$ to ∞, $s = -5m^2$ to ∞, and so on.

In the numerical S-matrix bootstrap literature, the analyticity constraints imposed are motivated by work from the 60s on axiomatic S-matrix theory [1]. Specifically, the "maximal analyticity" assumption is made, which states that the S-matrix is an analytic function of the Mandelstam variables on the physical sheet upto bound states and threshold cuts. Poles in the higher sheets are allowed by this assumption. The analytic structure of a 2d S-matrix is shown in fig.2.2. It is easy to check that eq.(2.6) maps the first sheet to the strip $0 \leq \text{Im } \theta \leq \pi$, and maps the branch cuts onto the boundaries of the said strip.

In this thesis, we are interested in theories with $O(N)$ symmetry. This symmetry allows us to write down the S-matrix as

$$S_{ab}^{cd}(\theta) = \delta_{ab}\delta^{cd}\sigma_A(\theta) + \delta_a^c\delta_b^d\sigma_T(\theta) + \delta_a^d\delta_b^c\sigma_R(\theta) \ , \tag{2.14}$$

where $\sigma_A(\theta)$, $\sigma_T(\theta)$ and $\sigma_R(\theta)$ are the annihilation, transmission and reflection amplitudes respectively. It's also useful to define the following isospin channels which diagonalize the unitarity constraint

$$S_I(\theta) = (N-1)S_A(\theta) + S_T(\theta) + S_R(\theta) \ , \tag{2.15}$$

$$S_-(\theta) = S_T(\theta) - S_R(\theta) \ , \tag{2.16}$$

$$S_+(\theta) = S_T(\theta) + S_R(\theta) \ , \tag{2.17}$$

where $S_I(\theta)$ is the $O(N)$ isospin singlet and $S_-(\theta)$ and $S_+(\theta)$ are the antisymmetric and symmetric channels. In terms of these S-matrix elements, the unitarity constraints are

$$|S_{\rm i}(\theta)|^2 \leq 1, \ \text{for i} = I, -, \text{and} \ + \ . \tag{2.18}$$

2.1 Exact results

The constraints stated above do not uniquely determine the S-matrix. However, in the case of integrable theories, we have an infinite set of symmetries and one can show that the multi-particle S-matrix can be factorized into a product of 2 particle S-matrices. Factorization implies a highly non-trivial cubic constraint on the S-matrix, which is obtained by considering the factorization of a $3 \to 3$ scattering into product of $2 \to 2$ S-matrices. This can be done in two ways as shown in fig.2.3 which must lead to the same result. So, we have the following constraint called the Yang-Baxter equation

$$S_{a_1a_2}^{c_1c_2}(\theta_1)S_{c_1a_3}^{b_1c_3}(\theta_1+\theta_2)S_{c_2c_3}^{b_2b_3}(\theta_2) = S_{a_2a_3}^{c_2c_3}(\theta_2)S_{a_1c_3}^{c_1b_3}(\theta_1+\theta_2)S_{c_1c_2}^{b_1b_2}(\theta_1) \ . \tag{2.19}$$

Another consequence of integrability is the absence of particle production i.e., the $2 \to 2$

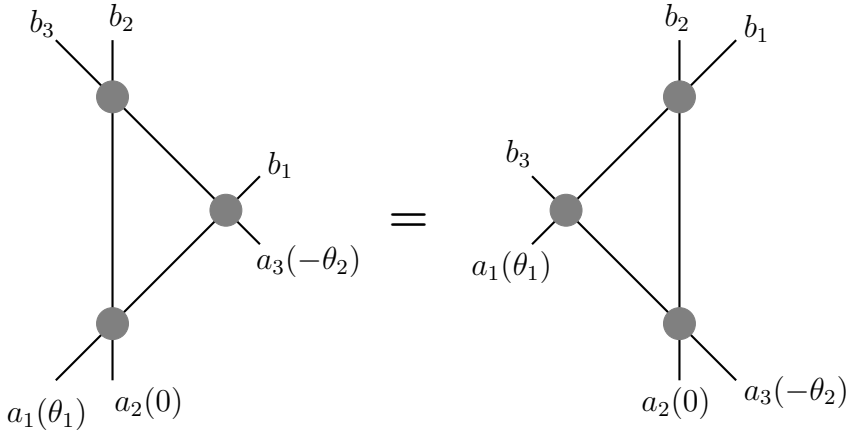

Figure 2.3. A pictorial depiction of the Yang-Baxter equation, which shows the equivalence of two ways of factorizing a $3 \to 3$ S-matrix into a product of $2 \to 2$ S-matrices. The indices of the intermediate particles are omitted.

S-matrix saturates the unitarity constraint. Once we include the factorization constraint and unitarity saturation, the S-matrices are restricted enough that we can compute them exactly. Several of these have been found in the literature including the integrable O(N) model, sinh-Gordon model, sine-Gordon model, various spin chain S-matrices etc. Here, we quote the results for the O(N) nonlinear sigma model (NLSM) and the periodic Yang-Baxter (pYB) solution.

2.1.1 $O(N)$ Nonlinear sigma model

This S-matrix corresponds to a physical model with N fields $\phi_a(x)$ with the following Lagrangian

$$\mathcal{L} = \frac{1}{2g}\partial_\mu\phi_a(x)\partial^\mu\phi_a(x) + \lambda(\phi_a(x)\phi_a(x) - 1) \ , \tag{2.20}$$

where g is a coupling constant and λ is a Lagrange multiplier which imposes the constraint that the vector $\phi_a(x)$ has unit length. This is a strongly coupled field theory and is a useful tool in studying QCD since it exhibits features like dynamical mass generation and asymptotic freedom [7]. NLSM can be solved perturbatively in the large N limit [32]. In [8], Zamolodchikov and Zamolodchikov obtained the exact S-matrix of the theory for finite N by solving the Yang-Baxter equation.

$$S_+^{NLSM}(\theta) = \frac{\theta - \mathrm{i}\lambda}{\theta + \mathrm{i}\lambda}\frac{\theta - \mathrm{i}\pi}{\theta + \mathrm{i}\pi}S_I^{NLSM}(\theta) \ , \tag{2.21a}$$

$$S_-^{NLSM}(\theta) = \frac{\theta - \mathrm{i}\pi}{\theta + \mathrm{i}\pi}S_I^{NLSM}(\theta) \ , \tag{2.21b}$$

$$S_I^{NLSM}(\theta) = -F_{\pi+\lambda}(\theta)F_{2\pi}(\theta) \ , \tag{2.21c}$$

where

$$\lambda = \frac{2\pi}{N-2} \ , \tag{2.22}$$

and the function $F_a(\theta)$ is defined as (see [9])

$$F_a(\theta) = \frac{\Gamma\left(\frac{a+\mathrm{i}\theta}{2\pi}\right)\Gamma\left(\frac{a-\mathrm{i}\theta}{2\pi}+\frac{1}{2}\right)}{\Gamma\left(\frac{a-\mathrm{i}\theta}{2\pi}\right)\Gamma\left(\frac{a+\mathrm{i}\theta}{2\pi}+\frac{1}{2}\right)} \ . \tag{2.23}$$

2.1.2 Periodic Yang-Baxter solution

This solution of the Yang-Baxter equation was discovered in [33] and later found through the S-matrix bootstrap in [34]. The transmission amplitude in this S-matrix is zero, and it exhibits periodicity to arbitrarily high energies. A physical model for this S-matrix is currently not known.

$$S_{+}^{pYB}(\theta) = H_{\nu/2}\left(\nu + \frac{\mathrm{i}\theta\nu}{\pi}, 2\nu - \frac{\mathrm{i}\theta\nu}{\pi}; \nu - \frac{\mathrm{i}\theta\nu}{\pi}, 2\nu + \frac{\mathrm{i}\theta\nu}{\pi}\right) , \tag{2.24a}$$

$$S_{-}^{pYB}(\theta) = -S_{+}^{pYB}(\theta) , \tag{2.24b}$$

$$S_{I}^{pYB}(\theta) = \frac{\sinh\left(\nu(1 - \frac{\mathrm{i}\theta}{\pi})\right)}{\sinh\left(\nu(1 + \frac{\mathrm{i}\theta}{\pi})\right)} S_{+}^{YB}(\theta) , \tag{2.24c}$$

with

$$H_{\nu}(\alpha, \beta; \gamma, \delta) = \lim_{N\to\infty} \prod_{\mathrm{j}=-N}^{N} \frac{\Gamma(\frac{\gamma+\mathrm{i}\pi\mathrm{j}}{4\nu})\Gamma(\frac{\delta+\mathrm{i}\pi\mathrm{j}}{4\nu})}{\Gamma(\frac{\alpha+\mathrm{i}\pi\mathrm{j}}{4\nu})\Gamma(\frac{\beta+\mathrm{i}\pi\mathrm{j}}{4\nu})} . \tag{2.25}$$

In this S-matrix, the parameter $\nu = \cosh^{-1}(N/2)$. We present another form of the function H_ν in appendix B which has better convergence in the infinite product. We also study some properties of this function which are useful in verifying the crossing constraint and the Yang-Baxter equation.

3. THE R-MATRIX - CONSTRAINTS AND EXACT RESULTS

In this chapter, we define the R-matrix in boundary QFTs and lay out the constraints that this quantity must obey. Once again, we need to define the asymptotic scattering states in the theory. In this case, for a theory defined on the right half line (see fig.3.3), we have left moving asymptotic in states which have well defined particle number at $t = -\infty$ and similarly, right moving out states which have well defined particle number at $t = +\infty$. We can parameterize the on shell momenta using eqns.(2.2) once again. We can now define the R-matrix for a theory with N particles with the same mass m, as the following amplitude

$$\mathbb{R}^{b_1,b_2,\dots}_{a_1,a_2,\dots}(\theta_{a_1},\theta_{b_1},\dots) = {}^{\text{out}}\langle b_1,\theta_{b_1};b_2,\theta_{b_2};\dots|a_1,\theta_{a_1};a_2,\theta_{a_2};\dots\rangle^{\text{in}} \ , \tag{3.1}$$

where the $a = 1 \dots N$ labels the particle flavor and the θ variables denote rapidities of the particles. The superscripts "in" and "out" indicate asymptotic in and out states. In this thesis, we shall only consider the $1 \to 1$ subsector of the reflection processes. Assuming that the boundary condition is time translation invariant, we see that the rapidity of the outgoing particle must be the negative of the rapidity of the incoming particle. We define the $1 \to 1$ R-matrix $R^b_a(\theta)$ as

$$R^b_a(\theta) = {}^{\text{out}}\langle\theta,b|-\theta,a\rangle^{\text{in}} \ . \tag{3.2}$$

As in the case of the S-matrix, the R-matrix must obey unitarity, analyticity and crossing constraints. Following the same argument as in section 2, we arrive at the following semidefinite unitarity constraint

$$RR^\dagger \preccurlyeq 1 \ . \tag{3.3}$$

The inequality accounts for possible particle production. Now, note that this constraint can be rewritten as the following condition

$$\begin{pmatrix} I & \hat{R} \\ \hat{R}^\dagger & I \end{pmatrix} \succcurlyeq 0 \ . \tag{3.4}$$

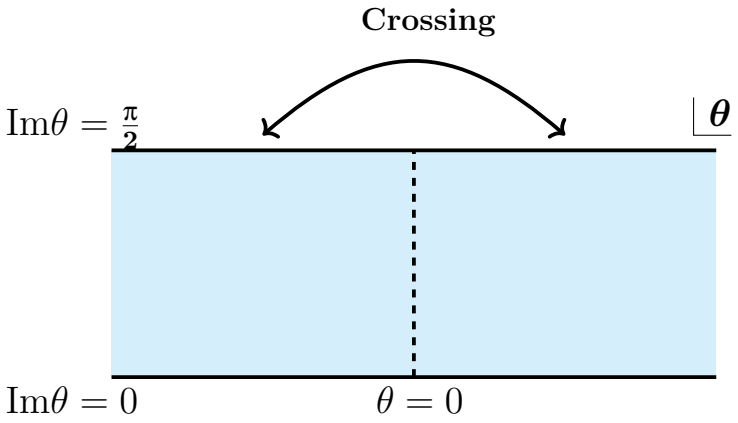

Figure 3.1. The R-matrix is analytic in the shaded region which corresponds to $\mathrm{Re}\,\varepsilon \geq 0$. The positive and negative real axes in the rapidity plane correspond to the data on the two sides of the branch cut. The crossing constraint eq.3.10 can be imposed at the boundary of the strip. We could have bound state poles on the dashed line along the imaginary axis. Resonances would appear as poles in the second sheet (with corresponding zeros in the physical sheet).

It is now easy to see that the unitarity constraint is convex because the space of positive semidefinite matrices is convex (i.e. if $M_1 \succcurlyeq 0$ and $M_2 \succcurlyeq 0$, then $\alpha M_1 + (1-\alpha)M_2 \succcurlyeq 0$ for all $\alpha \in [0,1]$). The convexity of this constraint facilitates the use of convex optimization methods as alluded to in the introduction.

Causality implies that the R-matrix has to be analytic in the region $\mathrm{Re}\,\varepsilon \geq 0$ which maps to the "physical strip" $0 \leq \mathrm{Im}\,\theta \leq \frac{\pi}{2}$, depicted in fig.3.1. As in the case of the S-matrix, there exist threshold branch cuts that are formed when the inelastic threshold is crossed i.e. we have sufficient energy for an intermediate particle to go on shell. Note that the first inelastic threshold for 1-to-1 R-matrices is at $\varepsilon = m$ (as opposed to $s = 4m^2$ for the S-matrix). We could also have additional branch cuts that correspond to more number of particles going on shell. Any bound states in the theory will show up as poles on the imaginary axis of the physical strip. In this thesis, we only consider theories without bound states poles. As in the case of the S-matrix, we can have resonances that show up as poles in the second sheet. Later on, we will impose a stricter constraint called extended analyticity, which requires the

R-matrix to be analytic in a larger region as in fig.3.2. This turns out to be a useful tool in better understanding the analytic structure of the allowed space of R-matrices.

Ghoshal and Zomolodchikov [35] introduced a crossing equation for boundary scattering in 2d theories. This crossing equation involves the bulk S-matrix which is assumed to be integrable. Consider 1+1d boundary QFT with space and time coordinates denoted by x and t. Let the theory be defined in the region $x \geq 0$. To derive the crossing equation, we first perform a double Wick rotation, $\tau = -\mathrm{i}x$, and $y = \mathrm{i}t$ that effectively swaps space and time (see fig.3.3). In these new coordinates, the boundary which was originally at $x = 0$ is now encoded in an initial state, say $|B\rangle$ of the theory at $\tau = 0$. The time evolution now is simply given by the bulk Hamiltonian. The quantity we are interested in is the $1 \to 1$ reflection amplitude which can be related to a pair creation process by the initial state $|B\rangle$. In the rest of this thesis, we will assume that the particles are their own anti-particles. Working through this transformation carefully, and using Hermitian analyticity, one can show that

$$^{\text{out}}\langle a, -\theta; b, \theta | B\rangle = R_a^b(\frac{\mathrm{i}\pi}{2} - \theta) \ , \tag{3.5}$$

$$^{\text{in}}\langle a, \theta; b, -\theta | B\rangle = R_a^b(\frac{\mathrm{i}\pi}{2} + \theta) \ . \tag{3.6}$$

Note that this is the sort of equation we would naively expect because boosts by an imaginary rapidity parameter is a rotation by that amount. Now, using the fact that the in-states form a complete basis, we can rewrite eq.(3.5) as

$$R_a^b(\frac{\mathrm{i}\pi}{2} - \theta) = \sum_{c_1, c_2, \ldots} \int \mathrm{d}\theta_1 \mathrm{d}\theta_2 \ldots \ ^{\text{out}}\langle a, -\theta; b, \theta | c_1, \theta_1, c_2, \theta_2, \ldots\rangle^{\text{in}} \ ^{\text{in}}\langle c_1, \theta_1, c_2, \theta_2, \ldots | B\rangle \ , \tag{3.7}$$

In an integrable theory, the intermediate states are restricted only to 2-particle states because of absence of particle production. Also, momentum conservation fixes the allowed rapidities of the intermediate states as follows

$$R_a^b(\frac{\mathrm{i}\pi}{2}-\theta) = \sum_{cd} {}^{\text{out}}\langle a,-\theta;b,\theta|d,\theta;c,-\theta\rangle^{\text{in}}\ {}^{\text{in}}\langle d,\theta;c,-\theta|B\rangle \ , \tag{3.8}$$

$$= S_{dc}^{ba}(2\theta)R_d^c(\frac{\mathrm{i}\pi}{2}+\theta) \ , \tag{3.9}$$

where in the second line, we used the definition of the 2-particle S-matrix. Now, using parity invariance of bulk S-matrix, we have

$$R_a^b(\frac{\mathrm{i}\pi}{2}-\theta) = S_{cd}^{ab}(2\theta)\, R_d^c(\frac{\mathrm{i}\pi}{2}+\theta) \ . \tag{3.10}$$

Note that we are only assuming integrability of the bulk S-matrix, not of the R-matrix. We can straightforwardly generalize this equation for when the bulk exhibits particle production starting from eq.(3.7). The crossing equation relates the values of the R-matrix on the positive imaginary axis ($\varepsilon = m\cosh(\frac{\mathrm{i}\pi}{2}+\theta)$) in the energy plane to those on the negative imaginary axis ($\varepsilon = m\cosh(\frac{\mathrm{i}\pi}{2}-\theta)$). Both these regions are on the boundary of the analyticity domain and so, we need to impose analyticity in a region at least as big as the physical strip to have a meaningful crossing constraint. Also, note that the analyticity of the R-matrix in the physical strip does not imply that it is also analytic in the region $\frac{\pi}{2} \leq \mathrm{Im}\,\theta \leq \pi$ because we can have additional poles from the S-matrix in eq.(3.10).

3.1 Exact Results

There are several R-matrices which have been exactly computed in the literature using integrability. By requiring that the boundary conditions preserve bulk integrability, we retain the property of factorization of scattering amplitudes. Assuming we have such an integrable boundary condition, we can factorize a $2 \to 2$ boundary reflection amplitude in two different

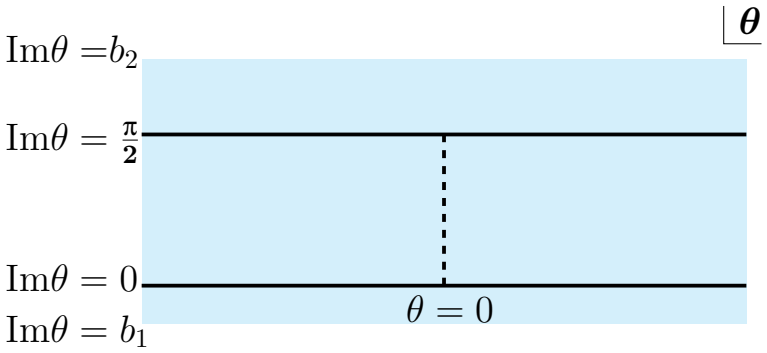

Figure 3.2. Extended analyticity constraint - we impose analyticity of the R-matrix in the shaded region $b_1 \leq \mathrm{Im}\,\theta \leq b_2$ where $b_1 \leq 0$ and $b_2 \geq \frac{\pi}{2}$

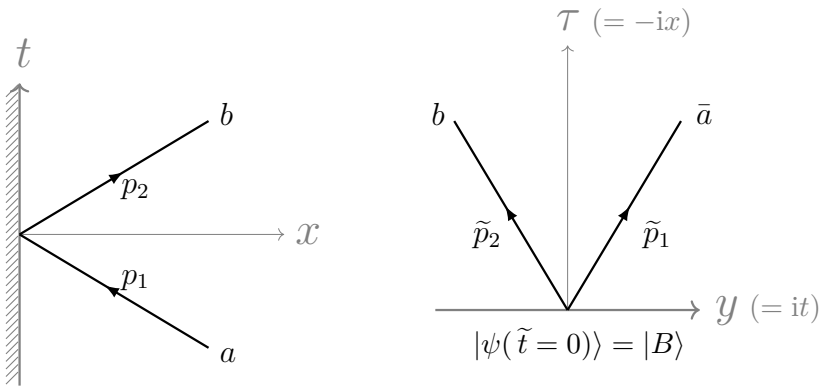

Figure 3.3. On the left, we have a $1 \to 1$ R-matrix for a particle a to reflect off the boundary into particle b. This amplitude is related to a pair creation process in the double Wick rotated frame as depicted on the right.

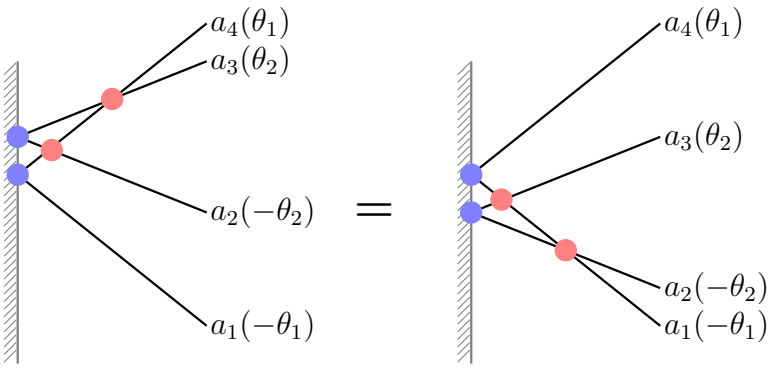

Figure 3.4. A pictorial depiction of the equivalence of the two ways of factorizing a $2 \to 2$ reflection process which yields the boundary Yang-Baxter equation. The blue circles denote $1 \to 1$ reflection processes and the red circles denote the bulk $2 \to 2$ S-matrix.

ways, shown in fig.3.4. Equating them, we get the boundary Yang-Baxter equation which reads

$$R^{c_1}_{a_1}(\theta_1) S^{c_2 c_3}_{c_1 a_2}(\theta_1+\theta_2) R^{c_4}_{c_3}(\theta_2) S^{a_3 a_4}_{c_4 c_2}(\theta_2-\theta_1) = S^{c_1 c_2}_{a_1 a_2}(\theta_2-\theta_1) R^{c_3}_{c_2}(\theta_2) S^{a_3 c_4}_{c_3 c_1}(\theta_1+\theta_2) R^{a_4}_{c_4}(\theta_1) \,. \quad (3.11)$$

In this section, we quote some exact results from the literature for theories with O(N) symmetry. Additionally, we present an analytic R-matrix for diagonal reflection for the periodic Yang Baxter model, which, to our knowledge, has not been worked out previously.

3.1.1 Diagonal ansatz for NLSM

In this subsection, we present an integrable R-matrix with NLSM in the bulk (see [36], [37] for this and related results). We pick the following ansatz for the R-matrix,

$$R = \text{diag}\{\underbrace{R_1(\theta), \ldots R_1(\theta)}_{k}, \underbrace{R_2(\theta) \ldots R_2(\theta)}_{N-k}\} \,. \quad (3.12)$$

where $k = 1 \dots N$. Clearly, this ansatz breaks the $O(N)$ symmetry of the bulk theory into $O(k) \times O(N-k)$. Plugging this ansatz into the crossing eq.(3.10), we get

$$R_1(\frac{\mathrm{i}\pi}{2} - \theta) = S_1(2\theta)R_1(\frac{\mathrm{i}\pi}{2} + \theta) + S_2(2\theta)R_2(\frac{\mathrm{i}\pi}{2} + \theta) \ , \tag{3.13a}$$

$$R_2(\frac{\mathrm{i}\pi}{2} - \theta) = S_3(2\theta)R_1(\frac{\mathrm{i}\pi}{2} + \theta) + S_4(2\theta)R_2(\frac{\mathrm{i}\pi}{2} + \theta) \ , \tag{3.13b}$$

where

$$S_1(\theta) = (N-k)S_A(\theta) + S_T(\theta) + S_R(\theta) \ , \qquad S_2(\theta) = k \ S_A(\theta) \ , \tag{3.14}$$

$$S_4(\theta) = k \ S_A(\theta) + S_T(\theta) + S_R(\theta) \ , \qquad S_3(\theta) = (N-k)S_A(\theta) \ . \tag{3.15}$$

Using this equation, in conjunction with the boundary Yang-Baxter equation, we get the following result [38]

$$R_1(\theta) = -R_0(\theta)F_{\frac{\lambda+\pi}{2}}(\theta)F_{\frac{\lambda(N-k-1)+\pi}{2}}(\theta) \ , \tag{3.16a}$$

$$R_2(\theta) = \frac{\frac{\lambda}{4}(N-2k) + \mathrm{i}\theta}{\frac{\lambda}{4}(N-2k) - \mathrm{i}\theta}R_1(\theta) \ , \tag{3.16b}$$

$$R_0(\theta) = \frac{\Gamma(\frac{1}{2} + \frac{\lambda}{4\pi} - \mathrm{i}\frac{\theta}{2\pi})\Gamma(1 + \mathrm{i}\frac{\theta}{2\pi})\Gamma(\frac{3}{4} + \frac{\lambda}{4\pi} + \mathrm{i}\frac{\theta}{2\pi})\Gamma(\frac{1}{4} - \mathrm{i}\frac{\theta}{2\pi})}{\Gamma(\frac{1}{2} + \frac{\lambda}{4\pi} + \mathrm{i}\frac{\theta}{2\pi})\Gamma(1 - \mathrm{i}\frac{\theta}{2\pi})\Gamma(\frac{3}{4} + \frac{\lambda}{4\pi} - \mathrm{i}\frac{\theta}{2\pi})\Gamma(\frac{1}{4} + \mathrm{i}\frac{\theta}{2\pi})} \ , \tag{3.16c}$$

where $\lambda = \frac{2\pi}{N-2}$ and $F_a(\theta)$ was defined in eq.(2.23). The case $k = N-1$ corresponds to Dirichlet boundary condition and $k = 0$ corresponds to Neumann boundary condition. These two special cases were solved in [38]. The R-matrices for the intermediate values of k were obtained in [37] and correspond to mixed boundary conditions.

3.1.2 Block diagonal ansatz for NLSM

In [37], the following block diagonal ansatz was considered for even N

$$R = \begin{pmatrix} A(\theta) & \mathrm{i}B(\theta) & 0 & 0 & \cdots \\ -\mathrm{i}B(\theta) & A(\theta) & 0 & 0 & \cdots \\ 0 & 0 & A(\theta) & \mathrm{i}B(\theta) & \cdots \\ 0 & 0 & -\mathrm{i}B(\theta) & A(\theta) & \cdots \\ \vdots & \vdots & \vdots & \vdots & \ddots \end{pmatrix} , \tag{3.17}$$

where $A(\theta)$ and $B(\theta)$ are real analytic functions, and we have the same 2×2 block repeated $N/2$ times along the diagonal. The alternating signs for off-diagonal terms are required by Hermitian analyticity. In this case, the crossing eq. (3.10) reduces to

$$A(\frac{\mathrm{i}\pi}{2} - \theta) = S_I(2\theta)A(\frac{\mathrm{i}\pi}{2} + \theta) \tag{3.18}$$

$$B(\frac{\mathrm{i}\pi}{2} - \theta) = -S_-(2\theta)B(\frac{\mathrm{i}\pi}{2} + \theta) \tag{3.19}$$

where S_I and S_- are the isospin singlet and antisymmetric channels.

The functions $A(\theta)$ and $B(\theta)$ can then be found using the bootstrap constraints along with the boundary Yang-Baxter equation to be

$$B(\theta) = -\mathrm{i}\alpha\theta A(\theta) \ , \tag{3.20a}$$

$$A(\theta) = \frac{1}{1 + \mathrm{i}\alpha\theta} F_{\frac{1}{\alpha}}(-\theta) R_0(\theta) \ . \tag{3.20b}$$

As we vary the free parameter α, we obtain a family of integrable R-matrices. This R-matrix has poles at $\theta = -\frac{\mathrm{i}}{\alpha}$ and $\theta = \mathrm{i}\pi + \frac{\mathrm{i}}{\alpha}$. This family of integrable models can be visualized by looking at a two dimensional slice, as in fig.5.4. The vertices occur as the poles move towards the physical strip in the limit $\alpha \to \infty$

3.1.3 Diagonal ansatz for pYB

In this subsection, we'll obtain an expression for the integrable, diagonal R-matrix with pYB in the bulk. To our knowledge, this R-matrix was not worked out previously in the literature. Once again, we'll start with the following diagonal ansatz

$$R = \text{diag}\{\underbrace{R_1(\theta),\dots R_1(\theta)}_{k},\underbrace{R_2(\theta)\dots R_2(\theta)}_{N-k}\}\ , \tag{3.21}$$

with $1 \leq k \leq N$. We can then plug this expression into the boundary Yang-Baxter eq.(3.11). Simplifying, and using the exact bulk S-matrix for pYB (2.24), we get

$$\frac{R_1(\theta)}{R_2(\theta)} = f(\theta) = \frac{\sin(\frac{\nu(\theta_0-\theta)}{\pi})\cos(\frac{\nu(\theta_0+\theta)}{\pi}+\mathrm{i}\alpha)}{\sin(\frac{\nu(\theta_0+\theta)}{\pi})\cos(\frac{\nu(\theta_0-\theta)}{\pi}+\mathrm{i}\alpha)}\ , \tag{3.22}$$

where $\alpha = \text{arctanh}\left(\frac{\cosh\nu-k}{\sinh\nu}\right)$. The constant $\theta_0 \in \mathrm{i}\mathbb{R}$ is not fixed by the boundary Yang-Baxter equation. Now, plugging in eq.(3.22) into the crossing eq.(3.10), we get

$$R_1(\mathrm{i}\pi-\theta) = \frac{h(\theta)}{h(\mathrm{i}\pi-\theta)}R_1(\theta) \tag{3.23}$$

with

$$h(\theta) = \frac{\sinh(\frac{2\mathrm{i}\theta\nu}{\pi})\prod_{n=-\infty}^{\infty}\Gamma\left(\frac{\mathrm{i}n\pi}{2\nu}-\frac{\mathrm{i}\theta}{\pi}\right)\Gamma\left(\frac{3}{2}+\frac{\mathrm{i}n\pi}{2\nu}+\frac{\mathrm{i}\theta}{\pi}\right)}{\sinh(\frac{\mathrm{i}\nu}{\pi}(\theta-\theta_0))\sinh(\frac{\mathrm{i}\nu}{\pi}(\theta+\theta_0)+\frac{\mathrm{i}\pi}{2}-\alpha)}\ . \tag{3.24}$$

Next, we need to impose unitarity constraint, which in the case of integrable R-matrices (which have no particle production) is $R_1(\theta)R_1(-\theta) = 1$, for $\theta \in \mathbb{R}$. It is useful to notice that the general solution to eq.(3.23) for real analytic $h(\theta)$, up to CDD factors [39], is

$$R_1(\theta) = \prod_{\mathrm{j}=0}^{\infty}\frac{h(-\mathrm{i}\pi+\theta-2\pi\mathrm{ij})h(-\theta-2\pi\mathrm{ij})}{h(-2\mathrm{i}\pi+\theta-2\pi\mathrm{ij})h(-\theta+\mathrm{i}\pi-2\pi\mathrm{ij})}\ . \tag{3.25}$$

Putting all this together, we get the following result

$$R_1(\theta) = \prod_{a=1}^{4} H_{\nu_a}\left(\frac{2\mathrm{i}\theta\nu_a}{\pi} + \alpha_a, -\frac{2\mathrm{i}\theta\nu_a}{\pi} + \beta_a; -\frac{2\mathrm{i}\theta\nu_a}{\pi} + \alpha_a, \frac{2\mathrm{i}\theta\nu_a}{\pi} + \beta_a\right) , \tag{3.26}$$

$$R_2(\theta) = \frac{R_1(\theta)}{f(\theta)} , \tag{3.27}$$

where $f(\theta)$ is defined in eq.(3.22), and the function H_ν in eq.(2.25). The parameters ν_a, β_a and α_a are as follows

$$\begin{aligned}
&\nu_1 = \frac{\nu}{2}, && \alpha_1 = \frac{\mathrm{i}\theta_0\nu}{\pi} + \frac{\mathrm{i}\pi}{2} - \alpha, && \beta_1 = \nu + \frac{\mathrm{i}\theta_0\nu}{\pi} + \frac{\mathrm{i}\pi}{2} - \alpha , \\
&\nu_2 = \frac{\nu}{2}, && \alpha_2 = -\frac{\mathrm{i}\theta_0\nu}{\pi}, && \beta_2 = \nu - \frac{\mathrm{i}\theta_0\nu}{\pi} , \\
&\nu_3 = \nu, && \alpha_3 = 2\nu, && \beta_3 = 0 , \\
&\nu_4 = \nu, && \alpha_4 = 3\nu, && \beta_4 = 2\nu .
\end{aligned} \tag{3.28}$$

One can easily check that this solution obeys the crossing equation (3.23) using the identities of the H_ν function given in appendix B. Also, note that this R-matrix is periodic with the same period as the bulk S-matrix, namely $R_{\mathrm{i}}(\theta) = R_{\mathrm{i}}(\theta + \frac{2\pi^2}{\nu})$. However, this solution has poles and common zeros in the physical region $0 \leq \mathrm{Im}\theta \leq \frac{\pi}{2}$ for certain values of θ_0 and thus is not a minimal solution. In order to eliminate them and obtain a minimal solution, we need to multiply the solution by appropriate prefactors called Castillejo-Dalitz-Dyson (CDD) factors [39] defined as,

$$f_{\mathrm{CDD}}(\theta;\alpha) = \frac{\sinh(\theta) - \sinh(\mathrm{i}\alpha)}{\sinh(\theta) + \sinh(\mathrm{i}\alpha)} . \tag{3.29}$$

Clearly, this function has poles at $\theta = -\mathrm{i}\alpha + 2n\pi\mathrm{i}$ and zeros at $\theta = \mathrm{i}\alpha + 2n\pi\mathrm{i}$, for $n \in \mathbb{Z}$. CDD factors satisfy the following two properties: (i) $|f_{\mathrm{CDD}}(\alpha,\theta)|^2 = 1$, and (ii) $f_{\mathrm{CDD}}(\alpha, \mathrm{i}\pi - \theta) = f_{\mathrm{CDD}}(\alpha,\theta)$. One can check that multiplying by such a prefactor preserves the integrability of an R-matrix. Let us now define a CDD factor that is periodic along the real axis as

$$f_P(\theta;\alpha) = \prod_{n=-\infty}^{\infty} \frac{\sinh(\theta + \frac{n\pi^2}{\nu}) - \sinh(\mathrm{i}\alpha)}{\sinh(\theta + \frac{n\pi^2}{\nu})\sinh(\mathrm{i}\alpha)} . \tag{3.30}$$

The periodic CDD factor has a periodicity of $\frac{2\pi^2}{\nu}$, however, the poles and zeros in it have a periodicity of $\frac{\pi^2}{\nu}$. Say $\theta_0 = 2\pi i\xi_0$, then we need to multiply our R-matrix with the following CDD factors as can be checked with some effort,

- if $\xi_0 < 0$ then $\alpha = 2\pi\left(\left\{\frac{1}{4} - \xi_0\right\} - \frac{1}{4}\right)$.
- if $\xi_0 > -\frac{\alpha}{2\nu}$ then $\alpha = 2\pi\left(\left\{\xi_0 + \frac{\alpha}{2\nu} + \frac{1}{4}\right\} - \frac{1}{4}\right)$.

where the curly braces denote the fractional part, defined by $\{\xi_0\} = \xi_0 - [\xi_0]$ (with $[\xi_0]$ being the largest integer smaller than or equal to ξ_0). Now, we can plot the coordinates $(R_1(\theta_1; \theta_0 = i\xi_0), R_2(\theta_1; \theta_0 = i\xi_0)$ as we vary $\xi_0 \in \mathbb{R}$, with θ_1 being a fixed point on the imaginary axis of the physical strip. We obtain the three solid curves of fig.5.6 corresponding to $k = 1, 2$ and 3, for $N = 6$. Once again, we have vertices along the curves whenever a new CDD factor needs to be included, i.e. at $\xi_0 = 0$ and $\xi_0 = -\frac{\alpha}{2\nu}$.

4. NUMERICAL SETUP AND THE DUAL PROBLEM

In this chapter, we will discuss how convex optimization tools can be used to solve the numerical R-matrix bootstrap and we'll also introduce the notion of convex duality which can be used as a check for our numerics. For the numerical bootstrap, the following class of problems will be of relevance

$$\begin{aligned} \max_{\hat{R}(\theta)} \quad & \mathcal{F}[\hat{R}(\theta)] \ , \\ \text{subject to:} \quad & \hat{R}\hat{R}^{\dagger} \preccurlyeq 1 \ , \\ & R_a^b\left(\frac{\mathrm{i}\pi}{2}-\theta\right) = S_{ab}^{cd}(2\theta) R_c^d\left(\frac{\mathrm{i}\pi}{2}+\theta\right) \ , \end{aligned} \tag{4.1}$$

where $\mathcal{F}$ is a linear functional of the variables and the maximization is done over the space of functions analytic in the strip $b_1 \leq \mathrm{Im}\,\theta \leq b_2$. Note that the crossing constraint is linear (for a fixed bulk S-matrix) and the unitarity constraint is convex, as discussed in section 2. Therefore, our problem is a bonafide convex optimization problem and we can tackle it numerically with very efficient solvers [40]–[42]. However, before we can plug this into a computer, we need to discretize the space of R-matrices. We do this by picking some ansatz for the R-matrices and then using a finite number of variables to parameterize the analytic matrix elements. We can then express the primal functional as a linear combination of the parameters. The crossing and unitarity constraints can be posed as simple linear and quadratic constraints. We've included the Python code for the bootstrap in appendix C.

4.1 Parameterizing analytic functions

In this section, we will discuss the discretization of the space of analytic functions in the strip $0 \leq \mathrm{Im}\theta \leq b$ (which is a simple translation of the general analyticity domain for the R-matrix elements $b_1 \leq \mathrm{Im}\,\theta \leq b_2$). There are several equivalent ways to do this - dispersion relations, Fourier series, spectral representations, etc. Here, we present the Fourier series parameterization which is one of the easiest to implement. Consider a function $f(\theta)$ analytic in the aforementioned strip and periodic along the real axis $f(\theta + 2a) = f(\theta)$. While most

R-matrices naturally are not periodic, we impose periodicity to facilitate the numerics by cutting off the energy range. We can expand this function as

$$f(\theta) = \sum_{n=-M}^{M} \tilde{f}_n \mathrm{e}^{\frac{\mathrm{i}n\pi\theta}{a}} \ , \tag{4.2}$$

where we truncate the series at some high-frequency cutoff $M \in \mathbb{N}$. The coefficients $\tilde{f}_n$ must be real when the function $f(\theta)$ is real analytic. Now, consider

$$f(\theta + \mathrm{i}b) = \tilde{f}_0 + \sum_{n=1}^{M} \left[\tilde{f}_n \mathrm{e}^{-\frac{n\pi b}{a}} \mathrm{e}^{\frac{\mathrm{i}n\pi\theta}{a}} + \tilde{f}_{-n} \mathrm{e}^{\frac{n\pi b}{a}} \mathrm{e}^{-\frac{\mathrm{i}n\pi\theta}{a}} \right] \ . \tag{4.3}$$

For large n, the last term gets exponentially large for coefficients $\tilde{f}_{-n}$ of $\mathcal{O}(1)$. To avoid numerical issues while working with large numbers, we multiply them by an exponential suppression factor as follows

$$\tilde{\tilde{f}}_n = \tilde{f}_{-n} \mathrm{e}^{-\frac{n\pi b}{\omega}} \ . \tag{4.4}$$

In terms of the new rescaled parameters, $f(\theta)$ is given by

$$f(\theta) = \tilde{f}_0 + \sum_{n=1}^{M} \tilde{f}_n \mathrm{e}^{\frac{\mathrm{i}n\pi\theta}{a}} + \tilde{\tilde{f}}_n \mathrm{e}^{-\frac{\mathrm{i}n\pi\theta}{a}} \ . \tag{4.5}$$

In this parameterization, we need to fix the values of M and a. Typically, we used values of M in the range 100 to 400. In cases where a pole approaches the analyticity domain, we need larger values of M in order to resolve such features. In order to deal with such situations, we increase the number of frequencies until the result of the optimization has converged. The periodicity a is chosen to be large enough that all the features of the R-matrix are clearly determined, taking into account that beyond $|\mathrm{Re}\,\theta| \sim \frac{a}{2}$, we notice unphysical boundary effects due to the imposed periodicity. The imaginary axis is farthest from the periodic boundary and therefore, the functions there are determined accurately.

4.2 Convex duality

In this section, we'll introduce the dual of a convex optimization problem. Before proceeding, let us define the notion of a convex cone - a vector space $\mathcal{K}$ is called a convex cone if $\forall\ v \in \mathcal{K},\ \alpha \in \mathbb{R}^+$, we have $\alpha v \in \mathcal{K}$. For a given convex cone $\mathcal{K}$, we can also define a dual convex cone $\mathcal{K}^*$ as

$$\mathcal{K}^* = \{\, s \mid s \cdot v \geq 0, \quad \forall\ v \in \mathcal{K} \,\} \ , \tag{4.6}$$

where the dot product is the usual Euclidean inner product. Now, in order to illustrate convex duality, consider the following convex optimization program

$$\max_{v_i} \quad \sum_{i=1}^{N} a_i v_i \ , \tag{4.7}$$

$$\text{subject to :} \quad \sum_{j=1}^{N} A_{ij} v_j + b_i = 0, \quad i = 1..M \ , \tag{4.8}$$

$$v_i \in \mathcal{K} \ , \tag{4.9}$$

where a_i are some coefficients that determine the primal functional, $\mathcal{K}$ is a convex cone, and we have certain equality constraints. Now, to obtain the dual problem, consider the following quantity, called the Lagrangian

$$\mathcal{L} = \sum_{i=1}^{N} a_i v_i + \sum_{i=1}^{N} \sum_{j=1}^{M} \lambda_j (A_{ji} v_i + b_j) + \sum_{i=1}^{N} s_i v_i \ , \tag{4.10}$$

where λ_i and s_i are called the dual variables. λ_i is simply a Lagrange multiplier which imposes the unitarity constraint, while s belongs to the dual cone $\mathcal{K}^*$. Note that that whenever v_i satisfies all the equality constraints and lies in the cone $\mathcal{K}$,

$$\mathcal{L} \geq \sum_{i=1}^{N} a_i v_i \ . \tag{4.11}$$

We can rewrite eq.(4.10) as

$$\mathcal{L} = \sum_{i=1}^{N} \left(a_i + \sum_{j=1}^{M} \lambda_j A_{ji} + s_i \right) v_i + \sum_{i=1}^{M} \lambda_i b_i \ . \tag{4.12}$$

We can now choose λ_i and s_i such that the coefficient of v_i is set to zero

$$a_i + \sum_{j=1}^{M} \lambda_j A_{ji} + s_i = 0 \ , \tag{4.13}$$

which implies

$$\mathcal{L} = \sum_{i=1}^{M} \lambda_i b_i \geq \sum_{i=1}^{N} a_i v_i \ . \tag{4.14}$$

We can now say that

$$\min_{\lambda_i, s_i} \left(\mathcal{F}_{\mathcal{D}} = \sum_{i=1}^{M} \lambda_i b_i \right) \geq \max_{v_i} \left(\mathcal{F}_{\mathcal{P}} = \sum_{i=1}^{N} a_i v_i \right) \ , \tag{4.15}$$

where $\mathcal{F}_{\mathcal{P}}$ and $\mathcal{F}_{\mathcal{D}}$ are called the primal and dual functionals respectively. The convex dual problem is now defined to be the minimization of $\mathcal{F}_{\mathcal{D}}$, subject to the constraint (4.13). The difference between the optimal primal functional and the optimal dual functional is called the duality gap. An important property of convex optimization problems is that the duality gap is zero whenever the dual problem is well posed [43]. In this manner, one can construct the dual problem for any primal problem of the type 4.1. However, in section 6, we present a much easier path to the dual problem which is also more intuitive. The two formulations of the dual problem can be shown to be equivalent [9].

5. RESULTS

Following the methods of the previous section, we bootstrapped R-matrices in the following cases - O(N) NLSM with diagonal and non diagonal reflections, and periodic Yang Baxter with diagonal reflection. The case of free theory in the bulk is considered in appendix A. The results obtained were verified using the convex dual problem introduced in section 4. In order to visualize the allowed space of R-matrices, we consider 2 dimensional sections of this infinite dimensional space and plot the boundary of the allowed region. For example we can take a point θ_1 on the imaginary axis and impose

$$R_1(\theta_1) = t\cos\alpha, \quad R_2(\theta_1) = t\sin\alpha \ , \tag{5.1}$$

where, $R_1(\theta)$ and $R_2(\theta)$ are two elements of the R-matrix and we and maximize t. We sweep through the values of α in the range $[0, 2\pi)$ and plot the corresponding $R_1(\theta_1)$ and $R_2(\theta_1)$. This gives us the projection of the boundary of allowed R-matrices in the 2d plane $R_1(\theta_1) - R_2(\theta_1)$, as seen in figs.5.1, 5.3, 5.4 and 5.6. In addition to obtaining this allowed region, we also have information about which functions $R_1(\theta)$ and $R_2(\theta)$ lie at the boundary.

We find integrable models at special points along the boundary of the convex domain and the R-matrices here agree excellently with the exact results of section 3. This provides a nontrivial test of the numerics.

5.1 NLSM, diagonal ansatz

We consider the following ansatz for the R-matrix:

$$R = \text{diag}\{\underbrace{R_1(\theta), \dots R_1(\theta)}_{k}, \underbrace{R_2(\theta) \dots R_2(\theta)}_{N-k}\} \ , \tag{5.2}$$

This R-matrix has a symmetry of $O(k) \times O(N-k)$. The functions $R_1(\theta)$ and $R_2(\theta)$ can be parameterized as described in section 4. We plot a 2 dimensional section of the allowed space of R-matrices by maximizing in various directions in the plane $R_1(\theta_1 = 0.2\text{i})$–$R_2(\theta_1 = 0.2\text{i})$ for the case $N = 6$ (i.e. the $O(6)$ model), assuming that these functions are analytic in the

strip $0 \leq \mathrm{Im}\,\theta \leq \frac{\pi}{2}$. For the case $k = 1$, the result is the outer curve of fig.5.1. Note that there are two vertices along the boundary of this region. The vertex marked by the red dashed circle agrees precisely with the integrable Dirichlet boundary condition of NLSM, as shown in fig.5.2. We do not know of any exact result that corresponds to the other vertex on the outer curve.

In order to explore this space of R-matrices further, we introduced the idea of extended analyticity, which is the assumption that the R-matrix is analytic in a region $b_1 \leq \mathrm{Im}\,\theta \leq b_2$ with $b_1 \leq 0$ and $b_2 > \frac{\pi}{2}$. We fix $b_1 = 0$ and vary b_2 in steps of 0.1. We find that The allowed region shrinks drastically at $b_2 = \frac{3\pi}{4}$ which corresponds to the exclusion of a pole at that $\theta = \frac{3\pi \mathrm{i}}{4}$. The allowed region then stays the same until we hit $b_2 = \boldsymbol{\pi}$. Beyond this, we set $b_1 = \boldsymbol{\pi} - b_2$ and increase $b_2 > \boldsymbol{\pi}$. The allowed region shrinks once more to exclude a pole at $\mathrm{i}\boldsymbol{\pi}$. In this manner, we can use the idea of extended analyticity to better explore the allowed regions. In fig.5.2, we plot the allowed region for $(b_1, b_2) = (0, 0.5\boldsymbol{\pi})$, $(0, 0.9\boldsymbol{\pi})$, and $(-0.1\boldsymbol{\pi}, 1.1\boldsymbol{\pi})$. It is interesting to note that the shape for $b_2 = 0.9\boldsymbol{\pi}$ has a new vertex (marked by a dashed purple circle in the figure) at which $R_1(\theta) = R_2(\theta)$ and also the boundary Yang Baxter equation is obeyed. This turned out to be the integrable Neumann boundary condition where $R_{\mathrm{i}}^{\mathrm{j}}(\theta) = \delta_{\mathrm{i}}^{\mathrm{j}} R(\theta)$.

We performed a similar analysis for the cases $O(2) \times O(4)$ and $O(3) \times O(3)$. These cases exhibit very similar behaviours with corresponding integrable vertices under extended analyticity, see fig.5.3.

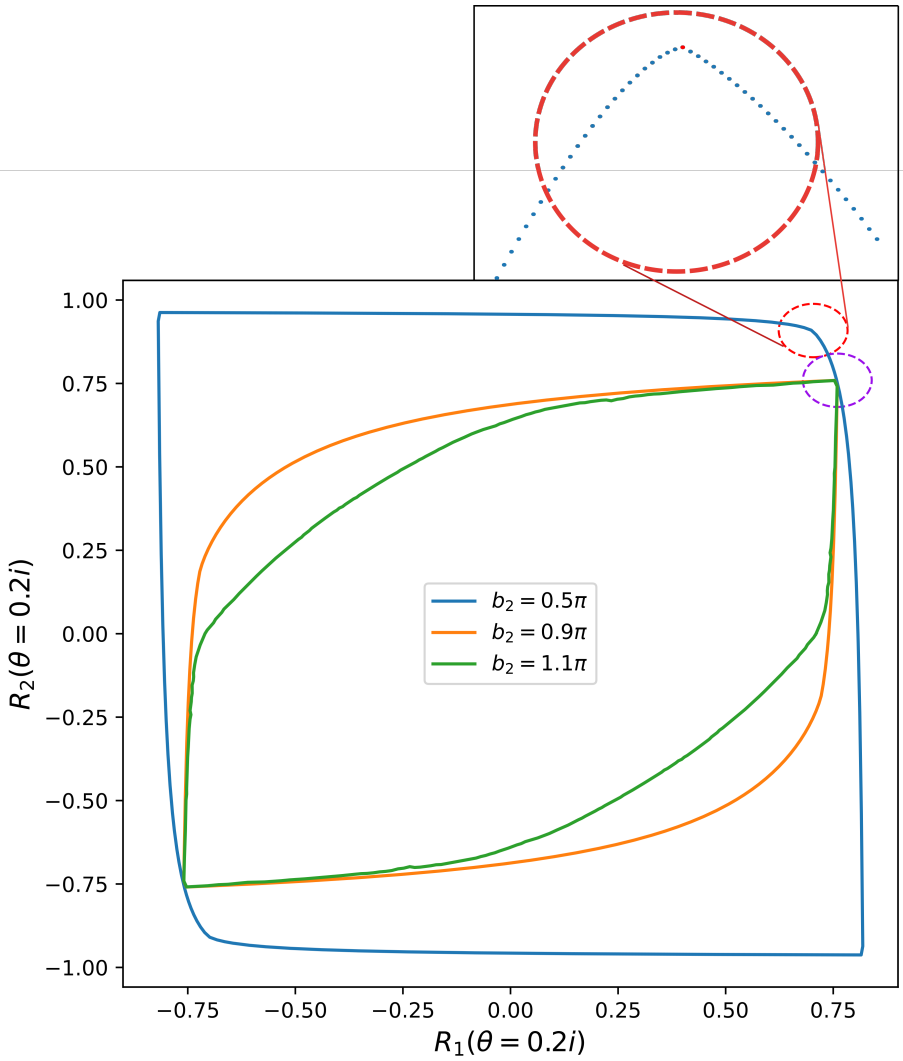

Figure 5.1. The three lines shown here correspond to $(b_1, b_2) = (0, 0.5\pi)$, $(0, 0.9\pi)$ and $(-0.1\pi, 1.1\pi)$ for NLSM with $N = 6, k = 1$. We can clearly see the drastic shrinking of the allowed region as we increase the domain of analyticity. The inset shows a rotated and rescaled boundary which makes the vertex more obvious. The vertex denoted by red is the Dirichlet boundary and the one in purple is Neumann boundary condition.

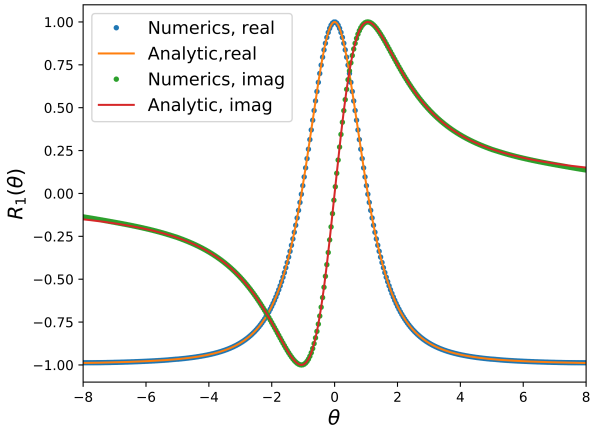

(a) $R_1(\theta)$, Dirichlet

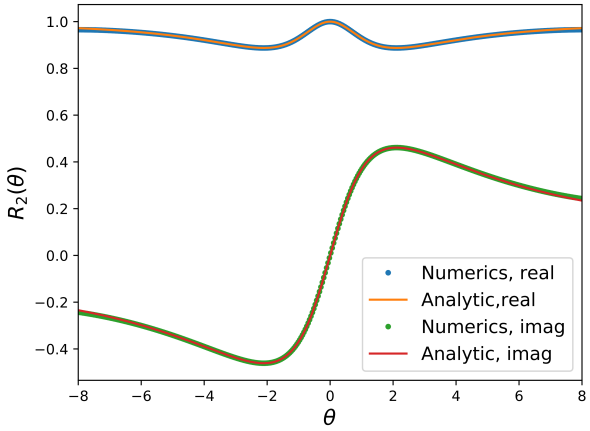

(b) $R_2(\theta)$, Dirichlet

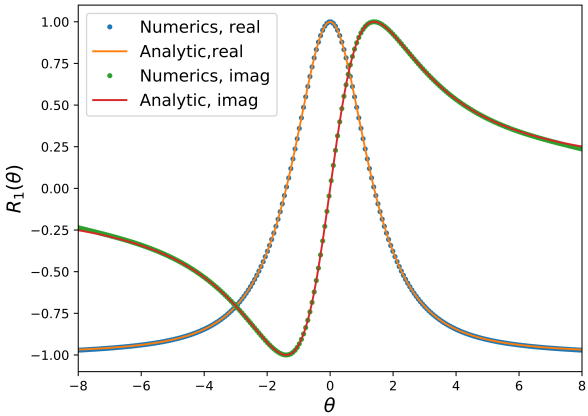

(c) $R_1(\theta)$, Neumann

Figure 5.2. Plot of $R_1(\theta)$ and $R_2(\theta)$ for θ on the real axis for the integrable vertices. Figs.(a) and (b) correspond to the red vertex of fig.5.1 which matches with the Dirichlet R-matrix while fig.(c) shows the agreement of purple vertex with the Neumann R-matrix (plot of $R_2(\theta)$ is omitted because at that vertex, $R_1(\theta) = R_2(\theta)$).

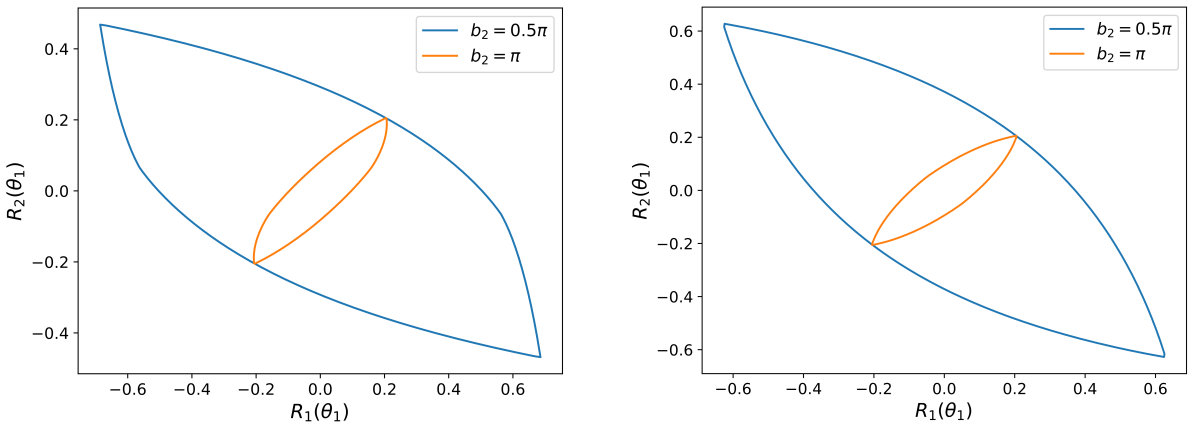

(a) $k = 2$ (b) $k = 3$

Figure 5.3. Plot of the allowed regions for NLSM with $N = 6$ and $k = 2, 3$ and $\theta_1 = 0.9879\text{i}$. As before, we have one integrable vertex for analyticity in the physical region, and extended analyticity an additional one

5.2 NLSM, block diagonal ansatz

Next, we bootstrapped a non-diagonal R-matrix, again with NLSM in the bulk. The following ansatz was chosen,

$$R = \begin{pmatrix} A(\theta) & \mathrm{i}B(\theta) & 0 & 0 & \cdots \\ -\mathrm{i}B(\theta) & A(\theta) & 0 & 0 & \cdots \\ 0 & 0 & A(\theta) & \mathrm{i}B(\theta) & \cdots \\ 0 & 0 & -\mathrm{i}B(\theta) & A(\theta) & \cdots \\ \vdots & \vdots & \vdots & \vdots & \ddots \end{pmatrix} , \tag{5.3}$$

with $A(\theta)$ and $B(\theta)$ being two analytic functions in the strip $0 \leq \mathrm{Im}\,\theta \leq \frac{\pi}{2}$. Once again, we plot the intersection of the allowed space of R-matrices with the plane $A(\theta_1 = 0.2\mathrm{i})$–$B(\theta_1 = 0.2\mathrm{i})$ in fig.5.4. Remarkably, the entire boundary of the allowed region corresponded to the integrable R-matrix described in section 3. In fig.5.4, we can see that the boundary of allowed region matches with eq.(3.20) as we vary the parameter α from 0 to ∞. The vertex in this figure corresponds to $\alpha \to \infty$, and in this limit, the poles at $\theta = -\frac{1}{\alpha}$ and $\theta = \boldsymbol{\pi} + \frac{1}{\alpha}$ approach the physical strip. Moreover, we plotted the components $A(\theta)$ and $B(\theta)$ for particular directions in fig.5.5 and the agreement with the integrable reflection is very precise.

5.3 Periodic Yang-Baxter, diagonal ansatz

Now, let us fix S-matrix in the bulk to be the pYB and pick the diagonal ansatz

$$R = \mathrm{diag}\{\underbrace{R_1(\theta), \ldots R_1(\theta)}_{k}, \underbrace{R_2(\theta) \ldots R_2(\theta)}_{N-k}\} \ . \tag{5.4}$$

We can again obtain the boundary of the allowed region in the $R_1(\theta_1) - R_2(\theta_1)$ plane for $k = 1, 2$ and 3 as shown in fig.5.6. The boundary agrees precisely with the integrable R-matrix of eq.(3.26) (after we include the appropriate CDD factors eq.(3.30)) as we vary the parameter $\theta_0 \in \mathrm{i}\mathbb{R}$. For any given point along the boundary, the numerical R-matrix is in

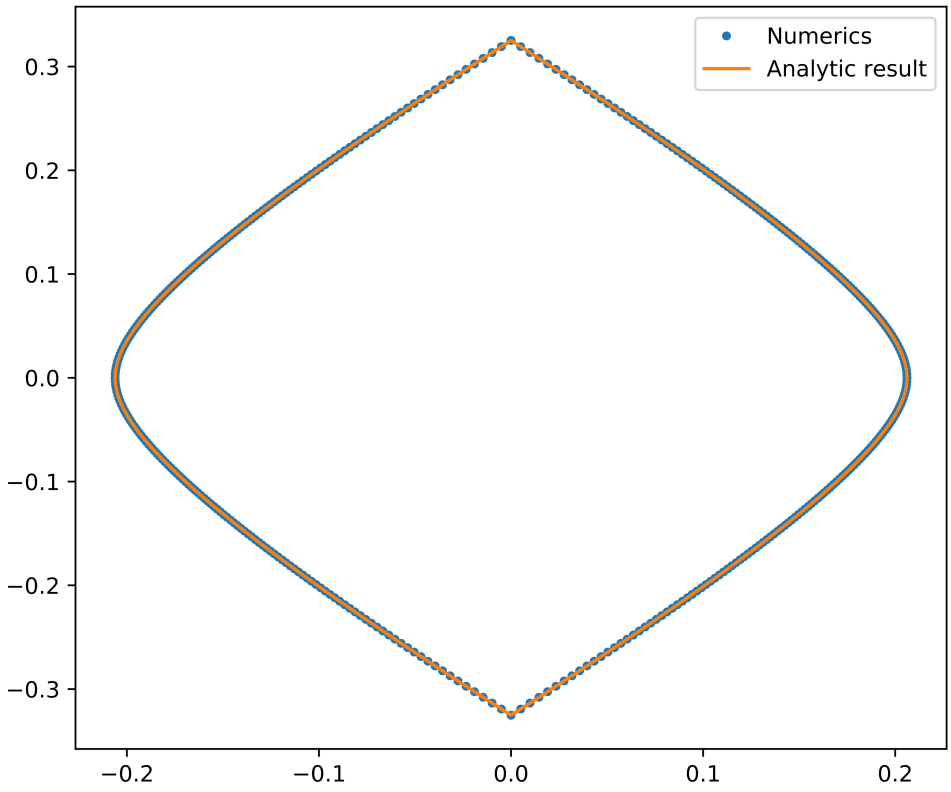

Figure 5.4. The allowed region in $A(\theta_1) - B(\theta_1)$ plane for $\theta_1 = 0.9879\,\mathrm{i}$ and NLSM in the bulk. The dots are the numerical results from the bootstrap, while the solid curve is the integrable R-matrix of eq.(3.20) for different values of the free parameter α.

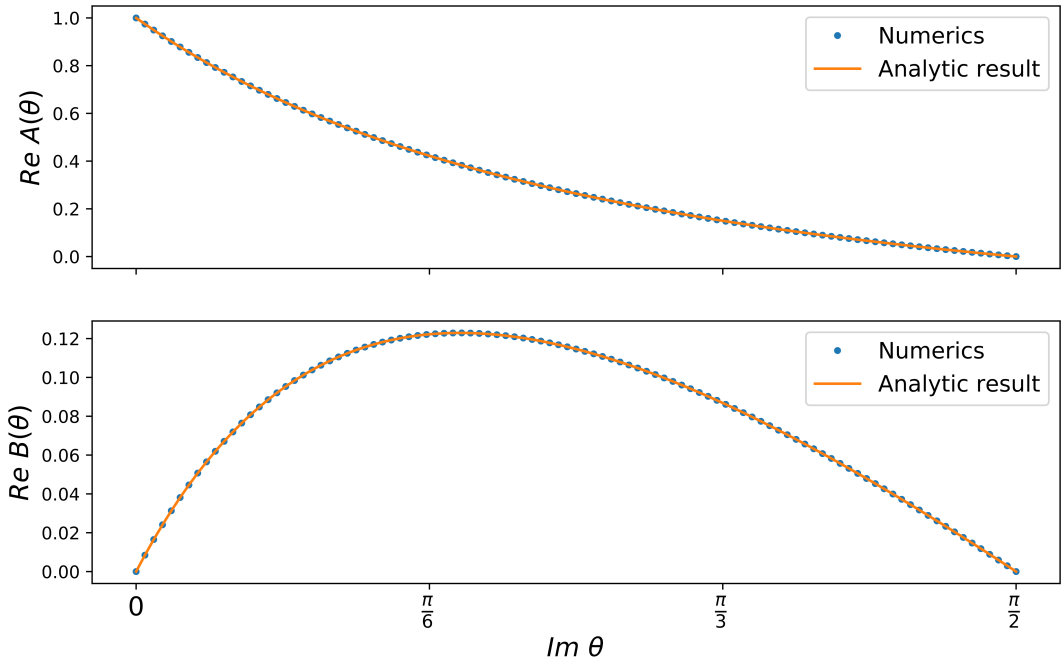

(a) The function $A(\theta)$ and $B(\theta)$ on the imaginary axis for $\alpha = 0.5$

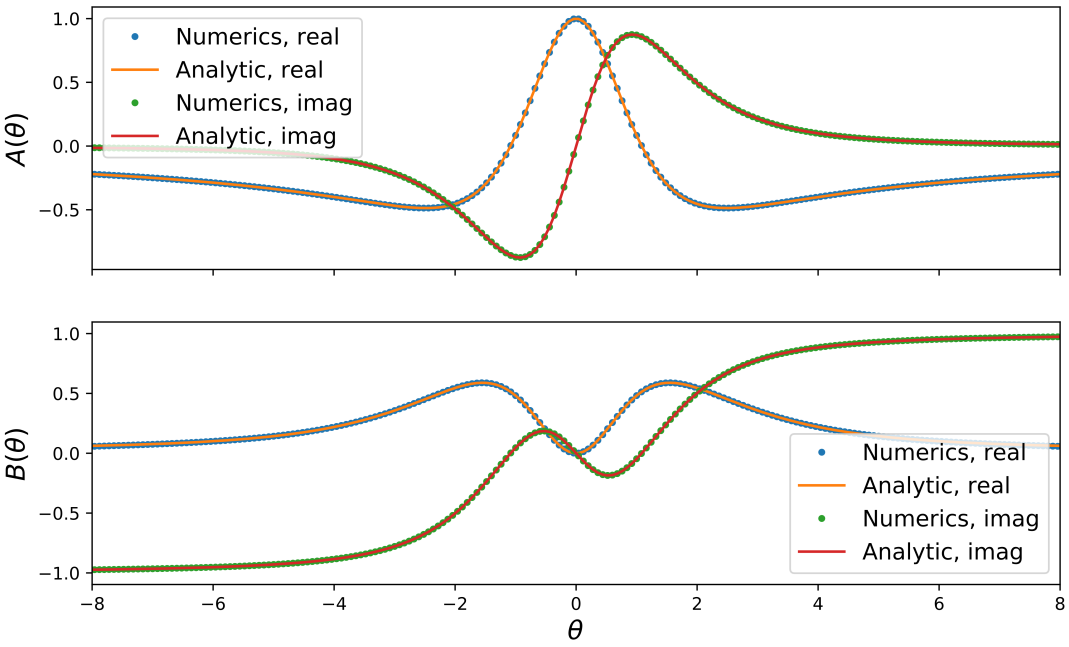

(b) The functions $A(\theta)$ and $B(\theta)$ on the real axis for $\alpha = 0.5$

Figure 5.5. Plot of $A(\theta)$ and $B(\theta)$ for θ along the real and imaginary axis of the physical strip for NLSM in the bulk and the off-diagonal ansatz for the R-matrix. We find that the numerical results and the integrable modes agree very well.

very good agreement with the exact result, as illustrated in fig.5.7. It is interesting to note that the vertices correspond to those values of θ_0 at which we need to change the CDD factor, namely $\xi_0 = 0, -\frac{\alpha}{2\nu}$. When $N = 6, k = 3$, we have $\alpha = \text{arctanh}(\frac{N/2-k}{\sinh\nu}) = 0$, and so we have only one vertex.

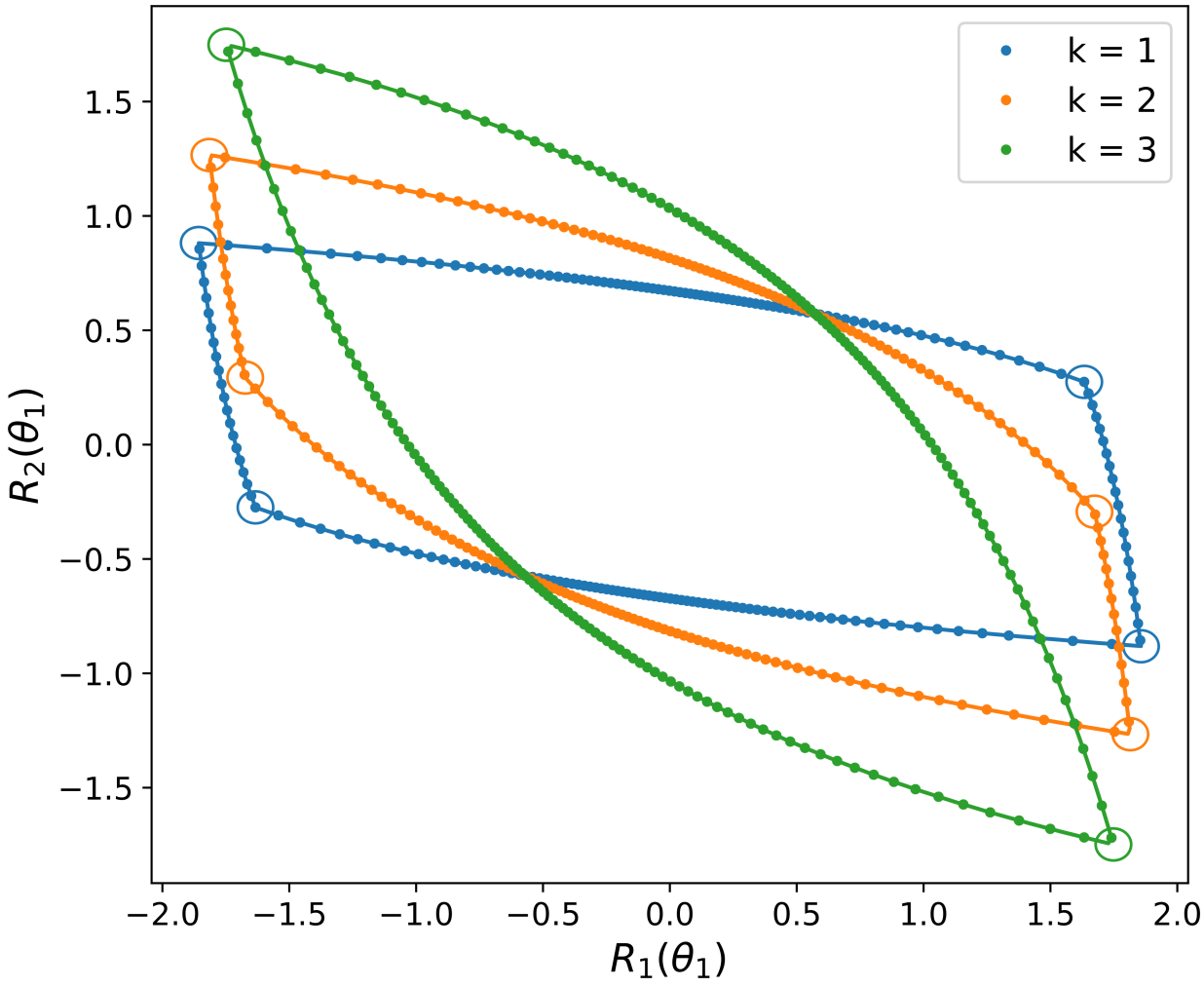

Figure 5.6. The allowed region for NLSM with $N = 6$, $k = 1, 2$ and 3, in the $R_1(\theta_1) - R_2(\theta_1)$ plane for $\theta_1 = 0.9879\text{i}$. The dots are the numerical result and the solid lines are the integrable R-matrix. The encircled vertices correspond to locations where the CDD factor changes. All the curves intersect at $R_1(\theta) = R_2(\theta)$ because this point is a common solution to all three cases.

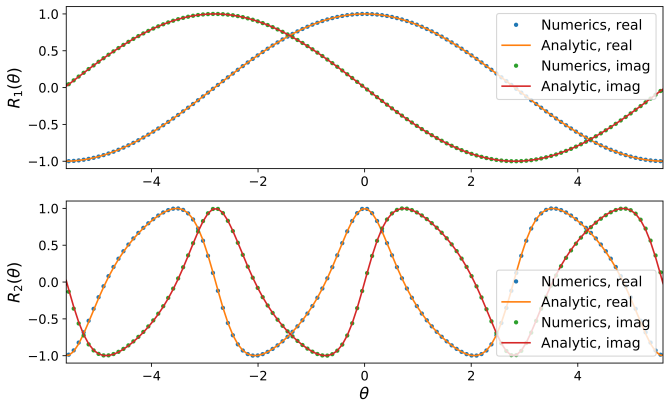

(a) $N = 6$, $k = 1$

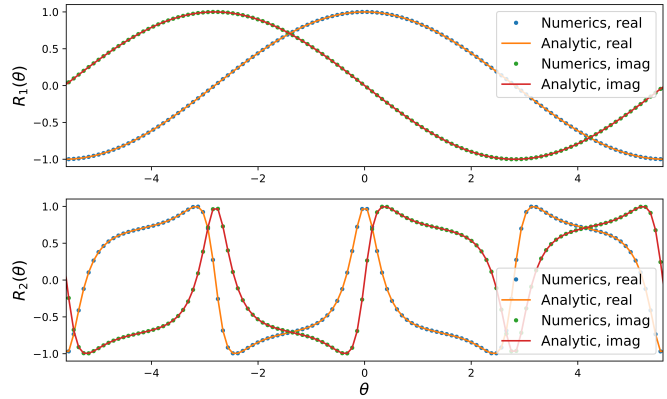

(b) $N = 6$, $k = 2$

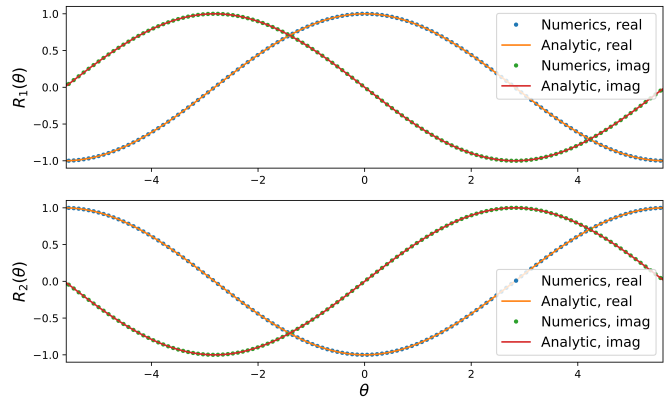

(c) $N = 6$, $k = 3$

Figure 5.7. This figure shows the agreement between the numerical and analytical R-matrices for $N = 6$, $k = 1, 2, 3$ and $\theta_0 = \frac{i\pi}{4}, -0.329i, 0$.

6. AN ALTERNATIVE DERIVATION OF THE DUAL PROBLEM

In this chapter, we discuss an alternative derivation of the dual problem using complex analysis which gives us an intuition for the dual constraints. We will first discuss the dual for the physical region, which is quite similar to the case of the S-matrix [9]. Then, we will present the dual for extended analyticity, where we find some new features. We do not provide numerical results for the dual problem because they agree with the primal results of the previous section.

6.1 The dual problem in the physical strip

The primal problem we considered in the previous sections involves constructing the R-matrices which satisfy the constraints and maximize the distance to the origin along various directions. As we increase the size of the basis for the primal variables, the allowed region expands and reaches the boundary from the inside. In the dual formulation of the problem, we instead exclude points that violate our constraints. So, as we increase the size of the basis, we approach the boundary from the outside and end up with the same allowed region [9]. Now, consider the the following primal functional to be maximized

$$\mathcal{F}_{\mathcal{P}} = \text{Re}\left[c_a^b R_b^a(\theta_1)\right] \ , \tag{6.1}$$

where c_a^b are some fixed real coefficients and θ_1 is any point in the region of analyticity ($0 \leq \text{Im}\,\theta \leq \frac{\pi}{2}$). Now, we can rewrite this functional as a contour integral by introducing dual analytic functions $K_a^b(\theta)$ which have a simple pole at $\theta = \theta_1$ with resides c_a^b,

$$\mathcal{F}_{\mathcal{P}} = \text{Re}\left[\frac{1}{2\pi\text{i}} \oint_{\mathcal{C}} d\theta R_b^a(\theta) K_a^b(\theta)\right] \ , \tag{6.2}$$

$$= \text{Re}\left[\frac{1}{2\pi\text{i}} \int_{-\infty}^{\infty} d\theta \left(R_b^a(\theta) K_a^b(\theta) - R_b^a(\frac{\text{i}\pi}{2} - \theta) K_a^b(\frac{\text{i}\pi}{2} - \theta)\right)\right] \ , \tag{6.3}$$

where $\mathcal{C}$ is a counterclockwise contour which encircles θ_1. In the second line, we expanded the contour until it hugs the boundary of the domain of analyticity and dropped the contribution from the vertical lines at infinity. Using the crossing equation (3.10), we get

$$\mathcal{F}_{\mathcal{P}} = \text{Re}\left[\frac{1}{2\pi\mathrm{i}}\int_{-\infty}^{\infty} d\theta \left(R_b^a(\theta)K_a^b(\theta) - S_{cd}^{ab}(2\theta)R_c^d(\frac{\mathrm{i}\pi}{2}+\theta)K_a^b(\frac{\mathrm{i}\pi}{2}-\theta)\right)\right] . \tag{6.4}$$

We now impose the following "anti-crossing constraint" on the dual functions $K_a^b(\theta)$

$$K_d^c(\frac{\mathrm{i}\pi}{2}+\theta) = -S_{cd}^{ab}(2\theta)K_a^b(\frac{\mathrm{i}\pi}{2}-\theta) . \tag{6.5}$$

Plugging this into eq.(6.4), and changing the integration variable for the second term $\theta \to -\theta$,

$$\mathcal{F}_{\mathcal{P}} = \text{Re}\left[\frac{1}{2\pi\mathrm{i}}\int_{-\infty}^{\infty} d\theta \left(R_b^a(\theta)K_a^b(\theta) + R_b^a(\frac{\mathrm{i}\pi}{2}-\theta)K_a^b(\frac{\mathrm{i}\pi}{2}-\theta)\right)\right] . \tag{6.6}$$

Adding eqns. (6.3) and (6.6), we get

$$\mathcal{F}_{\mathcal{P}} = \text{Re}\left[\frac{1}{2\pi\mathrm{i}}\int_{-\infty}^{+\infty} d\theta R_b^a(\theta)K_a^b(\theta)\right] . \tag{6.7}$$

When the R-matrix is diagonal, we can also choose diagonal $K_a^b(\theta)$. In that case, it is straightforward to put a bound on the right hand side, as in [9]. For more general R-matrices, we will use the von Neumann trace inequality [44] which reads

$$|\text{Tr}(AB)| \leq \sum_{\mathrm{i}} \alpha_{\mathrm{i}}\beta_{\mathrm{i}} , \tag{6.8}$$

where α_{i} and β_{i} are the singular values (arranged in decreasing order) of finite dimensional matrices A and B (recall that singular value decomposition of A is $A = U_1\Sigma_1 V_1^\dagger$ where U_1 and V_1 are unitary and Σ_1 is a diagonal matrix with the entries being the singular values). One can check that when this inequality is saturated, and the matrices A and B are non-singular [44],

$$V_2^\dagger U_1 = U_2^\dagger V_1 . \tag{6.9}$$

where U_1, V_1, U_2 and V_2 are the unitaries such that $A = U_1\Sigma_1 V_1^\dagger$ and $B = U_2\Sigma_2 V_2^\dagger$. Now, consider the following application of this inequality,

$$|\mathrm{Tr}(K(\theta)R(\theta))| \leq \sum_a k_a(\theta)\sigma_a(\theta) \ , \tag{6.10}$$

where $k_{\mathrm{i}}(\theta)$ are the singular values of $K_a^b(\theta)$ and $\sigma_{\mathrm{i}}(\theta)$ are those of $R_a^b(\theta)$. Using the unitarity constraint, we get[1] $\sigma_a(\theta) \leq 1$, which implies

$$|\mathrm{Tr}(K(\theta)R(\theta))| \leq \sum_a k_a(\theta) \ . \tag{6.11}$$

Putting all this together, we have

$$\begin{aligned}
\mathcal{F}_{\mathcal{P}} &= \mathrm{Re}\left[\frac{1}{2\pi \mathrm{i}}\int_{-\infty}^{+\infty} d\theta R_b^a(\theta)K_a^b(\theta)\right] \ , && (6.12)\\
&\leq \frac{1}{2\pi}\int_{-\infty}^{+\infty} d\theta\, |\mathrm{Tr}(R(\theta)K(\theta))| && (6.13)\\
&\leq \frac{1}{2\pi}\int_{-\infty}^{+\infty} d\theta \sum_{a=1}^{N} k_a(\theta) = \mathcal{F}_{\mathcal{D}} \ . && (6.14)
\end{aligned}$$

The right hand side of the last inequality is called the dual functional, and we define the dual problem to be the minimization of it subject to the anti-crossing constraint (6.5). When the R-matrix is diagonal, the dual functional is simply the sum of absolute values of the diagonal elements of $K_a^b(\theta)$ as we would expect. Conveniently, most convex optimization libraries include the Schatten 1-norm (also called the nuclear norm) which is precisely the sum of the singular values of a matrix, as in eq.(6.14).

In a convex optimization problem, the duality gap must go to zero. Therefore, at the optimal point, all the inequalities in this derivation must become equalities. Firstly, the equation $\sum_a k_a(\theta)\sigma_a(\theta) = \sum_a k_a(\theta)$ implies either $k_a(\theta) = 0$, or $\sigma_a(\theta) = 1$. Assuming that K

[1] ↑Say $R = \tilde{U}\tilde{\Sigma}\tilde{V}^\dagger$. We have $RR^\dagger = \tilde{U}\tilde{\Sigma}^2\tilde{U}^\dagger \preccurlyeq \mathbb{I}$ which implies $\sigma_a^2 \leq 1$

is invertible, the latter must be true. This then implies $RR^\dagger = R^\dagger R = \mathbb{I}$. Now, the saturation of the von Neumann trace inequality (6.9) along with unitarity saturation implies

$$R = \tilde{U}\mathbb{I}\tilde{V}^\dagger = \tilde{U}\tilde{U}^\dagger V U^\dagger \ , \tag{6.15}$$

$$= VU^\dagger \ . \tag{6.16}$$

where U and V are the unitaries such that $K = U\Sigma V^\dagger$. We verified that the R-matrix obtained this way matches the primal results. We also verified that the duality gap closes in all directions and we end up with the same allowed region.

6.2 The dual problem for extended analyticity

Here, we present a dual formulation of the extended analyticity problem. This case is quite interesting because it allows for unitarity non-saturation, as opposed to the dual in the physical region for both the S-matrix and the R-matrix bootstraps. Extending the domain of analyticity puts more constraints on the primal variables and so we end up with a smaller allowed region. As we'll see the dual for extended analyticity has more freedom than for the physical region and thus leads equivalently to a larger disallowed region.

As before, we start with the primal functional $\mathcal{F}_\mathcal{P} = \text{Re}\left[c_a^b R_b^a(\theta_1)\right]$ and rewrite it using analytic functions $K_a^b(\theta)$ which have a simple pole at $\theta = \theta_1$ with residue c_a^b. We then play the same contour games as before and impose anti-crossing constraint on $K_a^b(\theta)$ to arrive at,

$$\mathcal{F}_P = \text{Re}\left[\frac{1}{2\pi\mathrm{i}}\int_{-\infty}^{+\infty} d\theta \ K_a^b(\theta) R_a^b(\theta)\right] \ . \tag{6.17}$$

Let the extended analyticity constraint be that the R-matrix is analytic in the orange region of fig.6.1. To the right hand side of eq.(6.17), we add zero in the following form,

$$0 = \frac{1}{2\pi\mathrm{i}}\int_\mathcal{C} \tilde{K}_a^b(\theta) R_b^a(\theta) - \frac{1}{2\pi\mathrm{i}}\int_{-\infty}^{+\infty} \tilde{K}_a^b(\theta) R_b^a(\theta) \ , \tag{6.18}$$

where $\tilde{K}_a^b$ are functions analytic in the extended region (see fig.6.1). So, we have

$$\begin{aligned}\mathcal{F}_{\mathcal{P}} &= \mathrm{Re}\left[\frac{1}{2\pi \mathrm{i}}\int_{-\infty}^{+\infty} R_a^b(\theta)(K_b^a(\theta) - \tilde{K}_b^a(\theta))\right] + \mathrm{Re}\left[\frac{1}{2\pi \mathrm{i}}\int_{\mathcal{C}} \tilde{K}_b^a(\theta) R_a^b(\theta)\right] \\ &\leq \frac{1}{2\pi}\int_{-\infty}^{+\infty}\sum_a \Delta k_a + \mathrm{Re}\left[\frac{1}{2\pi \mathrm{i}}\int_{\mathcal{C}} \tilde{K}_b^a(\theta) R_a^b(\theta)\right] \ , \end{aligned} \tag{6.19}$$

where in the second line, we have used the von Neumann trace inequality and Δk_a are the singular values of ΔK with $\Delta K_a^b = K_a^b - \tilde{K}_a^b$. The second term of the last equation however cannot be bounded by unitarity. In order to do this, we introduce a regularization condition for the primal variables $R_a^b(\theta)$ on the curve $\mathcal{C}$, namely

$$RR^\dagger \preceq M \ , \tag{6.20}$$

where M is a real constant (multiplied by an $N \times N$ identity matrix). Now, we can proceed to write the dual functional as

$$\mathcal{F}_{\mathcal{D}} = \frac{1}{2\pi}\int_{-\infty}^{\infty}\sum_a \Delta k_a + \frac{M}{2\pi}\int_{\mathcal{C}} \tilde{k}_a(\theta)\left|\frac{d\theta(s\gamma)}{d\gamma}\right| d\gamma \ , \tag{6.21}$$

where $\theta(\gamma)$ is a parameterization of the curve $\mathcal{C}$ and $\tilde{k}_a(\theta)$ are the singular values of $\tilde{K}(\theta)$. We can interpret ΔK_a^b to be the jump across the real axis of single analytic function with a branch cut running from $-\infty$ to ∞ on the real axis. The first term of eq.(6.21) is then the integral of the jump across said cut.

Once again, at the optimal point, we must have zero duality gap. The analysis at this optimum remains the same as before but with K replaced by ΔK. When ΔK is invertible, we must have unitarity saturation. However, we could have unitarity non-saturation i.e. $\sigma_a(\theta) < 1$ as long as the corresponding $\Delta k_a(\theta) = 0$. This means that the singular values of K and $\tilde{K}$ are analytic continuations of each other through the real axis.

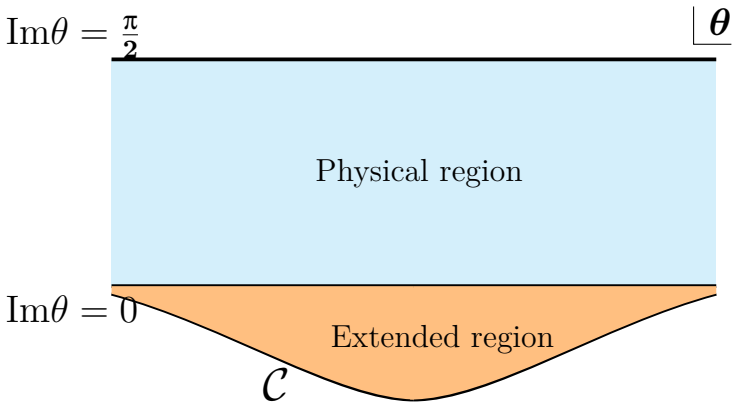

Figure 6.1. The extended analyticity constraint, where we extend the domain of analyticity upto some arbitrary curve $\mathcal{C}$ below the real axis. As described in the text, we need to regularize the R-matrix on the curve $\mathcal{C}$. The same analysis goes through for extended analyticity in the strip $b_1 \leq \mathrm{Im}\,\theta \leq b_2$ for $b_1 \leq 0$ and $b_2 \geq \frac{\pi}{2}$

7. CONCLUSIONS

We introduced an extension to the S-matrix bootstrap program to boundary QFTs and successfully reproduced known integrable R-matrices. We also introduced the extended analyticity constraint which allowed us to identify additional integrable models. This seems to be a promising way to study the allowed space of amplitudes and can be readily applied to the case of the S-matrix bootstrap (ongoing work). We also presented the dual to the extended analyticity problem and show that unlike the case where we have the standard analyticity domain, here, we can have theories which do not saturate unitarity as results of our optimization problem. We've only explored a few examples of boundary field theories with our bootstrap and this work can be extended in several ways, by investigating other theories including supersymmetric ones, theories with bound states, etc.

A. FREE THEORY

In this appendix, we obtain some analytic results for a free bulk S-matrix ($S_{\mathrm{ij}}^{kl} = \delta_{\mathrm{i}}^{k}\delta_{\mathrm{j}}^{l}$). In this case, one can check that the boundary Yang-Baxter equation is trivially satisfied. The crossing equation is simply

$$R_{\mathrm{i}}^{\mathrm{j}}(\mathrm{i}\boldsymbol{\pi} - \theta) = R_{\mathrm{j}}^{\mathrm{i}}(\theta) \ . \tag{A.1}$$

Now, we will obtain the space of allowed R-matrices for the diagonal (3.12) and block diagonal (3.17) ansatz.

In the diagonal case, we have two analytic functions $R_1(\theta)$ and $R_2(\theta)$ satisfy self crossing, i.e. $R_{\mathrm{i}}(\mathrm{i}\boldsymbol{\pi} - \theta) = R_{\mathrm{i}}(\theta)$ for $\mathrm{i} = 1, 2$, as can be seen from eq.(A.1). We also have the following unitarity constraints $|R_{\mathrm{i}}(\theta)| \leq 1$, for $\mathrm{i} = 1, 2$ and $\theta \in \mathbb{R}$. Self-crossing implies that the absolute value of the R-matrix is bounded by one along the entire boundary. So, the allowed region in $R_1(\theta_1) - R_2(\theta_1)$ plane for any θ_1 in the physical strip must be bounded by a square with vertices at $(\pm 1, \pm 1)$. These vertices themselves must be in the allowed region because the function $R_1(\theta) = \pm 1$ and $R_2(\theta) = \pm 1$ satisfy all the constraints. A property of convex spaces is that the convex hull of any subset of points must lie within the convex space itself. So, the allowed region must be bounded by the square with vertices at $(\pm 1, \pm 1)$ both from above and below. Therefore, we conclude that the allowed region is that said square itself. This result agrees with the numerics, as seen in fig.A.1.

In the block diagonal case (3.17), we also have two analytic functions $A(\theta)$ and $B(\theta)$ which, by crossing are equal to $A(\mathrm{i}\boldsymbol{\pi} - \theta)$ and $-B(\mathrm{i}\boldsymbol{\pi} - \theta)$ respectively. The primal maximization problem can be rewritten in terms of two new functions $u(\theta) = A(\theta) + B(\theta)$ and $v(\theta) = A(\theta) - B(\theta)$ as

$$\begin{aligned} \max_{u,v} \quad & \cos(\alpha)u(\theta_1) + \sin(\alpha)v(\theta_1) \ , \\ \text{s.t.} \quad & |u(\theta)| \leq 1, \quad |v(\theta)| \leq 1 \quad \text{for} \quad \theta \in \mathbb{R} \ , \\ & u(\mathrm{i}\boldsymbol{\pi} - \theta) = v(\theta) \ . \end{aligned} \tag{A.2}$$

We can solve this problem analytically by conformally mapping the strip $0 \leq \mathrm{Im}\ \theta \leq \boldsymbol{\pi}$ to the unit disk via $z(\theta) = \frac{\mathrm{i}-\mathrm{e}^{\theta}}{\mathrm{i}+\mathrm{e}^{\theta}}$. We can rewrite the optimization problem in terms of a single

analytic function $\tilde{u}(z(\theta)) = u(\theta)$ which satisfies $|\tilde{u}(z)| \leq 1$ on the unit circle ($|z| = 1$). This function has two poles located at $z(\theta_1)$ and at $-z(\theta_1)$. Using the result below eq.(12), page 138 of [45], the optimal function is of the form

$$\tilde{u}(z) = \frac{\mathrm{i}z + a}{1 + \mathrm{i}az} \ , \tag{A.3}$$

where a is real by real analyticity and lies in the range [-1,1]. As we sweep the angle α in the range $[0, 2\pi]$, we can check that the value of a covers the entire domain [-1,1] and therefore can be used to parameterize the boundary of the allowed region. Finally, the functions $A(\theta)$ and $B(\theta)$ at the boundary are given by

$$A(\theta) = \frac{2a\sinh(\theta)}{(a^2+1)\sinh(\theta) - \mathrm{i}(a^2-1)} \ , \tag{A.4}$$

$$B(\theta) = \frac{\mathrm{i}(a^2-1)\cosh(\theta)}{(a^2+1)\sinh(\theta) - \mathrm{i}(a^2-1)} \ . \tag{A.5}$$

Once again, we can check that this result agrees with the numerics for the block diagonal ansatz (see fig.A.1).

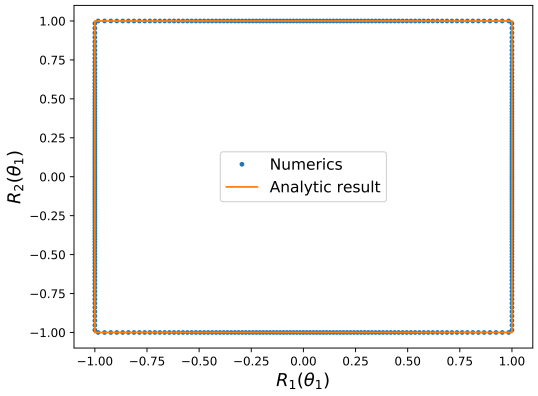

(a) Diagonal ansatz

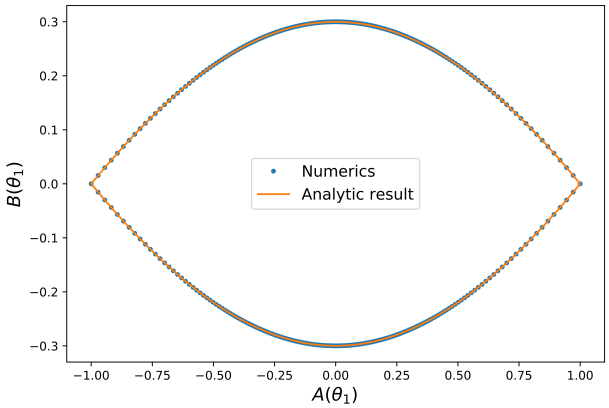

(b) Block diagonal ansatz

Figure A.1. The allowed region of R-matrices with free bulk for diagonal and block diagonal ansatz in excellent agreement with the numerics. In these plots, $\theta_1 = 0.9879\,\mathrm{i}$

B. A USEFUL FUNCTION

In this appendix, we define and discuss the properties of the function $H_\nu(\alpha,\beta;\gamma,\delta)$ which was introduced in the main body. Let α,β,γ and δ be four complex numbers that satisfy $\alpha+\beta=\gamma+\delta$ and $\nu\in\mathbb{R}_{>0}$. We define

$$H_\nu(\alpha,\beta;\gamma,\delta)=\lim_{N\to\infty}\prod_{\mathrm{j}=-N}^{N}\frac{\Gamma(\frac{\gamma+\mathrm{i}\pi\mathrm{j}}{4\nu})\Gamma(\frac{\delta+\mathrm{i}\pi\mathrm{j}}{4\nu})}{\Gamma(\frac{\alpha+\mathrm{i}\pi\mathrm{j}}{4\nu})\Gamma(\frac{\beta+\mathrm{i}\pi\mathrm{j}}{4\nu})} \tag{B.1}$$

$$=\mathrm{e}^{\frac{\alpha\beta-\gamma\delta}{4\nu}}\frac{(\mathrm{e}^{-2\beta},\mathrm{e}^{-8\nu})_\infty(\mathrm{e}^{-2\alpha},\mathrm{e}^{-8\nu})_\infty}{(\mathrm{e}^{-2\delta},\mathrm{e}^{-8\nu})_\infty(\mathrm{e}^{-2\gamma},\mathrm{e}^{-8\nu})_\infty}\ , \tag{B.2}$$

where we have introduced the q-Pochammer symbol $(a,q)_n=\prod_{\mathrm{j}=0}^{n}(1-aq^{\mathrm{j}})$. We can rewrite the function H_ν as

$$H_\nu(\alpha,\beta;\gamma,\delta)=\mathrm{e}^{\frac{\alpha\beta-\gamma\delta}{4\nu}}\prod_{\mathrm{j}=0}^{\infty}\frac{\sinh(\alpha+4\nu\mathrm{j})\sinh(\beta+4\nu\mathrm{j})}{\sinh(\gamma+4\nu\mathrm{j})\sinh(\delta+4\nu\mathrm{j})}\ , \tag{B.3}$$

where the infinite product is computed in the symmetric limit $\lim_{N\to\infty}\mathrm{j}=-N\dots N$. This function is analytic on the entire complex plane except for the presence of isolated poles and zeros. We have zeros when $\alpha=\mathrm{i}n\boldsymbol{\pi}-4\nu\mathrm{j}$ or $\beta=\mathrm{i}n\boldsymbol{\pi}-4\nu\mathrm{j}$ for all $n\in\mathbb{Z}$ and $\mathrm{j}\in\mathbb{N}\cup\{0\}$. Similarly, the function has poles when $\gamma=\mathrm{i}n\boldsymbol{\pi}-4\nu\mathrm{j}$ or $\delta=\mathrm{i}n\boldsymbol{\pi}-4\nu\mathrm{j}$ for all $n\in\mathbb{Z}$ and

$\mathrm{j} \in \mathbb{N} \cup \{0\}$. We now quote some simple identities of this function which are useful in checking the crossing and unitarity constraints of the diagonal R-matrix (3.26).

$$H_\nu(\alpha,\beta;\gamma,\delta) = H_\nu(\alpha,\beta;\delta,\gamma) = \frac{1}{H_\nu(\gamma,\delta;\alpha,\beta)} \ , \tag{B.4}$$

$$H_\nu(\alpha,\beta;\gamma,\delta) = H_\nu(\alpha,\beta;\mu,\rho)H_\nu(\mu,\rho;\gamma,\delta) \ , \tag{B.5}$$

$$H_\nu(\alpha+\mathrm{i}\pi,\beta+\mathrm{i}\pi;\gamma+\mathrm{i}\pi,\delta+\mathrm{i}\pi) = H_\nu(\alpha,\beta;\gamma,\delta) \ , \tag{B.6}$$

$$H_\nu(\alpha,\beta+\mathrm{i}\pi;\gamma,\delta+\mathrm{i}\pi) = \mathrm{e}^{\frac{\mathrm{i}\pi(\alpha-\gamma)}{4\nu}} H_\nu(\alpha,\beta;\gamma,\delta) \ , \tag{B.7}$$

$$H_\nu(\alpha,\beta;\gamma+\mathrm{i}\pi,\delta-\mathrm{i}\pi) = \mathrm{e}^{\frac{\mathrm{i}\pi(\gamma-\delta)}{4\nu}-\frac{\pi^2}{4\nu}} H_\nu(\alpha,\beta;\gamma,\delta) \ , \tag{B.8}$$

$$H_\nu(\alpha+4\nu,\beta+4\nu;\gamma+4\nu,\delta+4\nu) = \frac{\sinh\gamma\sinh\delta}{\sinh\alpha\sinh\beta} H_\nu(\alpha,\beta;\gamma,\delta) \ , \tag{B.9}$$

$$H_\nu(\alpha,\beta+4\nu;\gamma,\delta+4\nu) = \frac{\sinh\delta}{\sinh\beta} H_\nu(\alpha,\beta;\gamma,\delta) \ , \tag{B.10}$$

$$H_\nu(\alpha,\beta;\gamma+4\nu,\delta-4\nu) = \frac{\sinh\gamma}{\sinh(\delta-4\nu)} H_\nu(\alpha,\beta;\gamma,\delta) \ . \tag{B.11}$$

We also have the following doubling identity

$$H_\nu(\alpha,\beta;\gamma,\delta) = H_{2\nu}(\alpha+4\nu,\beta+4\nu;\gamma+4\nu,\delta+4\nu)H_{2\nu}(\alpha,\beta;\gamma,\delta) \ , \tag{B.12}$$

which can be derived from the Gamma function identity $\Gamma(2z) = \frac{2^{2z-1}}{\sqrt{\pi}}\Gamma(z)\Gamma(z+\frac{1}{2})$. In order to solve the crossing equation, it is useful to define the following function

$$\phi_{\alpha,\beta;\nu}(\theta) = H_\nu\left(\alpha+\frac{2\mathrm{i}\theta\nu}{\pi},\beta-\frac{2\mathrm{i}\theta\nu}{\pi};\alpha-\frac{2\mathrm{i}\theta\nu}{\pi},\beta+\frac{2\mathrm{i}\theta\nu}{\pi}\right) \ , \tag{B.13}$$

which satisfies

$$\phi_{\alpha,\beta;\nu}(\mathrm{i}\pi-\theta) = H_{\nu/2}\left(\alpha-\frac{2\mathrm{i}\theta\nu}{\pi}-2\nu,\beta+\frac{2\mathrm{i}\theta\nu}{\pi};\alpha+\frac{2\mathrm{i}\theta\nu}{\pi},\beta-\frac{2\mathrm{i}\theta\nu}{\pi}-2\nu\right)\phi_{\alpha,\beta;\nu}(\theta) \ . \tag{B.14}$$

In particular

$$\phi_{\alpha,\alpha+2\nu;\nu}(\mathrm{i}\pi-\theta) = \frac{\sinh(\alpha-\frac{2\mathrm{i}\theta\nu}{\pi}-2\nu)}{\sinh(\alpha+\frac{2\mathrm{i}\theta\nu}{\pi})}\phi_{\alpha,\alpha+2\nu;\nu}(\theta) \ , \tag{B.15}$$

can be used to solve the crossing equation (3.23) directly.

C. PYTHON CODE FOR THE R-MATRIX BOOTSTRAP

In this appendix, we include the code for our numerics which is written in the Python programming language. To get it running, one needs to install the "cvxpy" Python package and the "MOSEK" solver which offers free academic licenses. The following code computes the allowed region for NLSM in the bulk and a diagonal R-matrix ansatz with $N = 6$, $k = N - 1$.

```
from cvxpy import *
import numpy as np
import matplotlib.pyplot as plt
from scipy.special import gamma
from scipy.linalg import toeplitz

n = 100 #Number of variables
N = 6 #O(N) model
ap = 15
b1, b2 = 0, 0.5*np.pi

theta = ap/n * (np.arange(-n+0.5, n+0.5))
p1 = np.arange(1, n)

a1 = multiply(Variable(n-1), np.exp(p1*np.pi*b1/ap))
a2 = multiply(Variable(n-1), np.exp(p1*np.pi*b1/ap))
am1 = multiply(Variable(n-1), np.exp(-p1*np.pi*b2/ap))
am2 = multiply(Variable(n-1), np.exp(-p1*np.pi*b2/ap))
a01, a02 = Variable(), Variable()

def R1(theta):
    th, phi = np.real(theta), np.imag(theta)
    ktheta, kphi = 1j*np.pi/ap*np.outer(th, p1), np.pi/ap*np.outer(phi, p1)
    return a01 + np.exp(-kphi+ktheta) @ a1 + np.exp(kphi-ktheta) @ am1

def R2(theta):
    th, phi = np.real(theta), np.imag(theta)
    ktheta, kphi = 1j*np.pi/ap*np.outer(th, p1), np.pi/ap*np.outer(phi, p1)
    return a02 + np.exp(-kphi+ktheta) @ a2 + np.exp(kphi-ktheta) @ am2

def Q(theta):
    return gamma(1/(N-2) - 1j*theta/2/np.pi) / gamma(1/2 + 1/(N-2) - 1j*theta/2/np.pi) *\
    gamma(0.5 - 1j*theta/2/np.pi) / gamma(-1j*theta/2/np.pi)

def S_T(theta):
    return Q(theta) * Q(1j*np.pi-theta)

def S_A(theta):
    return -2j*np.pi/(N-2)/(1j*np.pi-theta) * Q(theta)*Q(1j*np.pi-theta)

def S_R(theta):
    return -2j*np.pi/(N-2)/theta * Q(theta)*Q(1j*np.pi-theta)

S1 = lambda theta: (N-1)*S_A(theta)+S_R(theta)+S_T(theta)
S2 = lambda theta: S_A(theta)
S3 = lambda theta: (N-1)*S_A(theta)
S4 = lambda theta: S_A(theta)+S_R(theta)+S_T(theta)

```

```
R11, R21 = R1(theta), R2(theta)

constraints = []
# Unitarity
constraints += [abs(R11) <= 1, abs(R21) <= 1]

# Crossing upper bdy
Rp_th = 1j*b2 + theta
Rm_th = 1j*np.pi - Rp_th
cross_th = Rp_th - Rm_th

constraints += [R1(Rm_th) == multiply(R1(Rp_th), S1(cross_th)) + multiply(R2(Rp_th), S2(cross_th))]
constraints += [R2(Rm_th) == multiply(R1(Rp_th), S3(cross_th)) + multiply(R2(Rp_th), S4(cross_th))]

tol = 1e-6
mosek_params = {"MSK_DPAR_INTPNT_CO_TOL_PFEAS":tol, "MSK_DPAR_INTPNT_CO_TOL_DFEAS":tol, "
    MSK_DPAR_INTPNT_CO_TOL_REL_GAP":tol}
cos_a, sin_a = Parameter(), Parameter()

pt1_3j, pt2_3j = R1(0.2j), R2(0.2j)

t = cos_a * real(pt1_3j) + sin_a * real(pt2_3j)
constraints += [sin_a*real(pt1_3j) == cos_a*real(pt2_3j)]

objective = Maximize(t)
prob = Problem(objective, constraints)

Nalpha = 100
alphaV = np.linspace(0, np.pi, Nalpha)
plot_R1, plot_R2 = np.zeros(Nalpha), np.zeros(Nalpha)

for i, alpha in enumerate(alphaV):
    cos_a.value, sin_a.value = np.cos(alpha), np.sin(alpha)
    try:
        prob.solve(solver=MOSEK, mosek_params=mosek_params, verbose=False)
        plot_R1[i], plot_R2[i] = real(pt1_3j).value, real(pt2_3j).value
        print(alpha, plot_R1[i], plot_R2[i])
    except:
        print("didnt work")
        plot_R1[i], plot_R2[i]= np.nan, np.nan

x = np.append(plot_R1, -plot_R1)
y = np.append(plot_R2, -plot_R2)
```

REFERENCES

[1] R. J. Eden, P. V. Landshoff, D. I. Olive, and J. C. Polkinghorne, *The analytic S-matrix*. Cambridge: Cambridge Univ. Press, 1966.

[2] M. F. Paulos, J. Penedones, J. Toledo, B. C. van Rees, and P. Vieira, "The S-matrix bootstrap. Part I: QFT in AdS," *JHEP*, vol. 11, p. 133, 2017. DOI: 10.1007/JHEP11(2017)133. arXiv: 1607.06109 [hep-th].

[3] M. F. Paulos, J. Penedones, J. Toledo, B. C. van Rees, and P. Vieira, "The S-matrix bootstrap II: two dimensional amplitudes," *JHEP*, vol. 11, p. 143, 2017. DOI: 10.1007/JHEP11(2017)143. arXiv: 1607.06110 [hep-th].

[4] M. F. Paulos, J. Penedones, J. Toledo, B. C. van Rees, and P. Vieira, "The S-matrix bootstrap. Part III: higher dimensional amplitudes," *JHEP*, vol. 12, p. 040, 2019. DOI: 10.1007/JHEP12(2019)040. arXiv: 1708.06765 [hep-th].

[5] A. Homrich, J. Penedones, J. Toledo, B. C. van Rees, and P. Vieira, "The S-matrix Bootstrap IV: Multiple Amplitudes," *JHEP*, vol. 11, p. 076, 2019. DOI: 10.1007/JHEP11(2019)076. arXiv: 1905.06905 [hep-th].

[6] Y. He, A. Irrgang, and M. Kruczenski, "A note on the S-matrix bootstrap for the 2d O(N) bosonic model," *JHEP*, vol. 11, p. 093, 2018. DOI: 10.1007/JHEP11(2018)093. arXiv: 1805.02812 [hep-th].

[7] A. M. Polyakov, "Interaction of Goldstone Particles in Two-Dimensions. Applications to Ferromagnets and Massive Yang-Mills Fields," *Phys. Lett. B*, vol. 59, pp. 79–81, 1975. DOI: 10.1016/0370-2693(75)90161-6.

[8] A. B. Zamolodchikov and A. B. Zamolodchikov, "Factorized s Matrices in Two-Dimensions as the Exact Solutions of Certain Relativistic Quantum Field Models," *Annals Phys.*, vol. 120, I. M. Khalatnikov and V. P. Mineev, Eds., pp. 253–291, 1979. DOI: 10.1016/0003-4916(79)90391-9.

[9] L. Córdova, Y. He, M. Kruczenski, and P. Vieira, "The O(N) S-matrix Monolith," *JHEP*, vol. 04, p. 142, 2020. DOI: 10.1007/JHEP04(2020)142. arXiv: 1909.06495 [hep-th].

[10] C. Bercini, M. Fabri, A. Homrich, and P. Vieira, "S-matrix bootstrap: Supersymmetry, Z_2, and Z_4 symmetry," *Phys. Rev. D*, vol. 101, no. 4, p. 045 022, 2020. DOI: 10.1103/PhysRevD.101.045022. arXiv: 1909.06453 [hep-th].

[11] Y. He and M. Kruczenski, "S-matrix bootstrap in 3+1 dimensions: regularization and dual convex problem," Mar. 2021. arXiv: 2103.11484 [hep-th].

[12] J. Elias Miró, A. L. Guerrieri, A. Hebbar, J. Penedones, and P. Vieira, "Flux Tube S-matrix Bootstrap," *Phys. Rev. Lett.*, vol. 123, no. 22, p. 221 602, 2019. DOI: 10.1103/PhysRevLett.123.221602. arXiv: 1906.08098 [hep-th].

[13] A. L. Guerrieri, J. Penedones, and P. Vieira, "Bootstrapping QCD Using Pion Scattering Amplitudes," *Phys. Rev. Lett.*, vol. 122, no. 24, p. 241 604, 2019. DOI: 10.1103/PhysRevLett.122.241604. arXiv: 1810.12849 [hep-th].

[14] S. Caron-Huot, D. Mazac, L. Rastelli, and D. Simmons-Duffin, "Sharp Boundaries for the Swampland," Feb. 2021. arXiv: 2102.08951 [hep-th].

[15] A. Guerrieri, J. Penedones, and P. Vieira, "Where is String Theory?," Feb. 2021. arXiv: 2102.02847 [hep-th].

[16] A. Guerrieri, J. Penedones, and P. Vieira, "S-matrix Bootstrap for Effective Field Theories: Massless Pions," Nov. 2020. arXiv: 2011.02802 [hep-th].

[17] A. L. Guerrieri, A. Homrich, and P. Vieira, "Dual S-matrix bootstrap. Part I. 2D theory," *JHEP*, vol. 11, p. 084, 2020. DOI: 10.1007/JHEP11(2020)084. arXiv: 2008.02770 [hep-th].

[18] A. Hebbar, D. Karateev, and J. Penedones, "Spinning S-matrix Bootstrap in 4d," Nov. 2020. arXiv: 2011.11708 [hep-th].

[19] C. Behan, L. Di Pietro, E. Lauria, and B. C. Van Rees, "Bootstrapping boundary-localized interactions," *JHEP*, vol. 12, p. 182, 2020. DOI: 10.1007/JHEP12(2020)182. arXiv: 2009.03336 [hep-th].

[20] Y.-t. Huang, J.-Y. Liu, L. Rodina, and Y. Wang, "Carving out the Space of Open-String S-matrix," Aug. 2020. arXiv: 2008.02293 [hep-th].

[21] S. Komatsu, M. F. Paulos, B. C. Van Rees, and X. Zhao, "Landau diagrams in AdS and S-matrices from conformal correlators," *JHEP*, vol. 11, p. 046, 2020. DOI: 10.1007/JHEP11(2020)046. arXiv: 2007.13745 [hep-th].

[22] H. Elvang, "Bootstrap and Amplitudes: A Hike in the Landscape of Quantum Field Theory," Jul. 2020. arXiv: 2007.08436 [hep-th].

[23] A. Bose, P. Haldar, A. Sinha, P. Sinha, and S. S. Tiwari, "Relative entropy in scattering and the S-matrix bootstrap," *SciPost Phys.*, vol. 9, p. 081, 2020. DOI: 10.21468/SciPostPhys.9.5.081. arXiv: 2006.12213 [hep-th].

[24] M. Correia, A. Sever, and A. Zhiboedov, "An Analytical Toolkit for the S-matrix Bootstrap," Jun. 2020. arXiv: 2006.08221 [hep-th].

[25] D. Karateev, S. Kuhn, and J. Penedones, "Bootstrapping Massive Quantum Field Theories," *JHEP*, vol. 07, p. 035, 2020. DOI: 10.1007/JHEP07(2020)035. arXiv: 1912.08940 [hep-th].

[26] P. Nayak, R. R. Poojary, and R. M. Soni, "A Note on S-Matrix Bootstrap for Amplitudes with Linear Spectrum," Jul. 2017. arXiv: 1707.08135 [hep-th].

[27] A. Sever and A. Zhiboedov, "On Fine Structure of Strings: The Universal Correction to the Veneziano Amplitude," *JHEP*, vol. 06, p. 054, 2018. DOI: 10.1007/JHEP06(2018)054. arXiv: 1707.05270 [hep-th].

[28] N. Doroud and J. Elias Miró, "S-matrix bootstrap for resonances," *JHEP*, vol. 09, p. 052, 2018. DOI: 10.1007/JHEP09(2018)052. arXiv: 1804.04376 [hep-th].

[29] C. Behan, "Bootstrapping the long-range Ising model in three dimensions," *J. Phys. A*, vol. 52, no. 7, p. 075 401, 2019. DOI: 10.1088/1751-8121/aafd1b. arXiv: 1810.07199 [hep-th].

[30] P. D. Anderson and M. Kruczenski, "Loop Equations and bootstrap methods in the lattice," *Nucl. Phys. B*, vol. 921, pp. 702–726, 2017. DOI: 10.1016/j.nuclphysb.2017.06.009. arXiv: 1612.08140 [hep-th].

[31] L. Chim, "Boundary S matrix for the tricritical Ising model," *Int. J. Mod. Phys. A*, vol. 11, pp. 4491–4512, 1996. DOI: 10.1142/S0217751X9600208X. arXiv: hep-th/9510008.

[32] E. Brezin and J. Zinn-Justin, "Spontaneous Breakdown of Continuous Symmetries Near Two-Dimensions," *Phys. Rev. B*, vol. 14, p. 3110, 1976. DOI: 10.1103/PhysRevB.14.3110.

[33] M. Hortacsu, B. Schroer, and H. J. Thun, "A Two-dimensional σ Model With Particle Production," *Nucl. Phys. B*, vol. 154, pp. 120–124, 1979. DOI: 10.1016/0550-3213(79)90374-2.

[34] L. Córdova and P. Vieira, "Adding flavour to the S-matrix bootstrap," *JHEP*, vol. 12, p. 063, 2018. DOI: 10.1007/JHEP12(2018)063. arXiv: 1805.11143 [hep-th].

[35] S. Ghoshal and A. B. Zamolodchikov, "Boundary S matrix and boundary state in two-dimensional integrable quantum field theory," *Int. J. Mod. Phys. A*, vol. 9, pp. 3841–3886, 1994, [Erratum: Int.J.Mod.Phys.A 9, 4353 (1994)]. DOI: 10.1142/S0217751X94001552. arXiv: hep-th/9306002.

[36] I. Aniceto, Z. Bajnok, T. Gombor, M. Kim, and L. Palla, "On integrable boundaries in the 2 dimensional $O(N)$ σ-models," *J. Phys. A*, vol. 50, no. 36, p. 364 002, 2017. DOI: 10.1088/1751-8121/aa8205. arXiv: 1706.05221 [hep-th].

[37] M. Moriconi, "Integrable boundary conditions and reflection matrices for the O(N) nonlinear sigma model," *Nucl. Phys. B*, vol. 619, pp. 396–414, 2001. DOI: 10.1016/S0550-3213(01)00527-2. arXiv: hep-th/0108039.

[38] S. Ghoshal, "Boundary S matrix of the O(N) symmetric nonlinear sigma model," *Phys. Lett. B*, vol. 334, pp. 363–368, 1994. DOI: 10.1016/0370-2693(94)90701-3. arXiv: hep-th/9401008.

[39] L. Castillejo, R. H. Dalitz, and F. J. Dyson, "Low's scattering equation for the charged and neutral scalar theories," *Phys. Rev.*, vol. 101, pp. 453–458, 1956. DOI: 10.1103/PhysRev.101.453.

[40] Michael Grant and Stephen Boyd, *"CVX: Matlab software for disciplined convex programming"*, version 2.0 beta, Sep. 2013. [Online]. Available: http://cvxr.com/cvx.

[41] M. C. Grant and S. P. Boyd, "Graph implementations for nonsmooth convex programs," in *Recent Advances in Learning and Control*, V. D. Blondel, S. P. Boyd, and H. Kimura, Eds., London: Springer London, 2008, pp. 95–110, ISBN: 978-1-84800-155-8.

[42] A. Nemirovski, "Advances in convex optimization: Conic programming," *Proceedings oh the International Congress of Mathematicians, Vol. 1, 2006-01-01, ISBN 978-3-03719-022-7, pags. 413-444*, vol. 1, Jan. 2006. DOI: 10.4171/022-1/17.

[43] R. J. Duffin, "Clark's theorem on linear programs holds for convex programs," *Proceedings of the National Academy of Sciences*, vol. 75, no. 4, pp. 1624–1626, 1978, ISSN: 0027-8424. DOI: 10.1073/pnas.75.4.1624. eprint: https://www.pnas.org/content/75/4/1624.full.pdf. [Online]. Available: https://www.pnas.org/content/75/4/1624.

[44] L. Mirsky, "A trace inequality of john von neumann.," eng, *Monatshefte für Mathematik*, vol. 79, pp. 303–306, 1975. [Online]. Available: http://eudml.org/doc/177697.

[45] "Chapter 8 - extremal problems," in *Theory of Hp Spaces*, ser. Pure and Applied Mathematics, P. L. Duren, Ed., vol. 38, Elsevier, 1970, pp. 129–146. DOI: https://doi.org/10.1016/S0079-8169(08)62672-0. [Online]. Available: https://www.sciencedirect.com/science/article/pii/S0079816908626720.